LIPOPROTEIN(a) WITH AN INTACT LYSINE BINDING SITE PROTECTS THE RETINA FROM AN AGE-RELATED MACULAR DEGENERATION PHENOTYPE IN MICE (AN AMERICAN OPHTHALMOLOGICAL SOCIETY THESIS)

By James T. Handa MD, Mizuki Tagami MD, Katayoon Ebrahimi MD, Gregor Leibundgut MD, Anna Janiak PhD, Joseph L. Witztum MD, and Sotirios Tsimikas MD

ABSTRACT

Purpose: To test the hypothesis that the accumulation of oxidized phospholipids (OxPL) in the macula is toxic to the retina unless neutralized by a variety of mechanisms, including binding by lipoprotein(a) [Lp(a)], which is composed of apolipoprotein(a) [apo(a)] and apolipoprotein B-100 (apoB).

Methods: Human maculas and eyes from two Lp(a) transgenic murine models were subjected to morphologic, ultrastructural, and immunohistochemical analysis. "Wild-type Lp(a)" mice, which express human apoB-100 and apo(a) that contains oxidized phospholipid, and "mutant LBS$^-$ Lp(a)" mice with a defective apo(a) lysine binding site (LBS) for oxidized phospholipid binding, were fed a chow or high-fat diet for 2 to 12 months. Oxidized phospholipid–containing lipoproteins were detected by immunoreactivity to E06, a murine monoclonal antibody binding to the phosphocholine headgroup of oxidized, but not native, phospholipids.

Results: Oxidized phospholipids, apo(a), and apoB accumulate in maculas, including drusen, of age-related macular degeneration (AMD) samples and age-matched controls. Lp(a) mice fed a high-fat diet developed age-related changes. However, mutant LBS$^-$ Lp(a) mice fed a high-fat diet developed retinal pigment epithelial cell degeneration and drusen. These changes were associated with increased OxPL, decreased antioxidant defenses, increased complement, and decreased complement regulators.

Conclusions: Human maculas accumulate Lp(a) and OxPL. Mutant LBS$^-$ Lp(a) mice, lacking the ability to bind E06-detectable oxidized phospholipid, develop AMD-like changes. The ability of Lp(a) to bind E06-detectable OxPL may play a protective role in AMD.

Trans Am Ophthalmol Soc 2015;113:T5[1-22].

INTRODUCTION

Oxidative stress has been theorized to play a substantive role in the development of age-related macular degeneration (AMD), the most common cause of blindness among the elderly in Western societies. While oxidation reactions are essential parts of metabolism and signal transduction, inadequately neutralized reactive oxygen species can damage lipids, proteins, and DNA.[1] In part, they do this by initiating lipid peroxidation, which leads to generation of oxidized lipids and oxidized lipid-protein adducts. We have shown that such oxidation-specific epitopes (OSEs) are proinflammatory and are recognized by both adaptive and innate immune responses.[2,3] Inadequate neutralization of the OSEs can convert the protective immune reaction into a pathologic response. For example, we have shown that the complement regulator factor H, which is classically known to control the alternative pathway, also binds the lipid peroxidation product malondialdehyde (MDA), and that the 402H polymorphism, which confers increased risk for AMD, has reduced binding to MDA, indicating a causal link to disease etiology.[4]

Oxidation-specific epitopes have been identified in all layers of the macula in AMD. In the retina, docosohexanoic acid, the most abundant fatty acid in photoreceptor tips, is oxidized to carboxyethylpyrrole (CEP) as well as other oxidized lipids, which "tag" oxidatively damaged photoreceptors in AMD.[5,6] The retinal pigment epithelium (RPE) contains multiple OSEs, including MDA and 4-hydroxynonenal, as well as advanced glycation end products (AGEs),[7,8] whereas Bruch's membrane, including drusen, contains AGEs, MDA, CEP, and oxidized phospholipids (OxPL).[6,9-11] We are especially interested in OxPL, not only because they are a prominent consequence of lipid peroxidation of the highly polyunsaturated fatty acids found in the photoreceptors, but also because OxPL are prominently formed when cells undergo apoptosis, a known mechanism of cell death in AMD.[12] As studied in this thesis, the term *OxPl* refers to phosphocholine (PC)-containing OxPL, which we detect with the IgM natural antibody E06 that binds to the PC moiety of OxPL but not to the PC moiety of unoxidized phospholipids.[13,14]

The Curcio laboratory has identified an age-dependent accumulation of low-density lipoprotein (LDL)–like particles in Bruch's membrane with aging and AMD.[15-18] We identified similar, oxidized lipoprotein particles in Bruch's membrane, including drusen, in early AMD samples and found that oxidized LDL (OxLDL) induced a pathologic response to RPE cells in vitro.[19] Oxidized lipoproteins contain a variety of products resulting from oxidative modifications to both the lipid and apolipoprotein components.[20] This work prompted our interest in lipoprotein (a) [Lp(a)], which is a lipoprotein composed of apolipoprotein(a) [apo(a)] covalently bound to apolipoprotein B-100 (apoB) by a disulfide bond between Cys4326 of apoB and Cys4057 of apo(a) on kringle IV type 9 (KIV9).[21-23] Apo(a) is highly homologous to the plasminogen gene, which contains 5 kringles (K) and a protease domain. However, apo(a) is distinct from plasminogen, as it contains only KIV (10 subtypes, of which KIV-2 is present in multiple and variable copies) and KV, and has an inactive protease domain due to a Ser^{561}-Ile^{562} substitution for Arg^{561}-Val^{562} that prevents plasminogen activators

From the Wilmer Eye Institute, Johns Hopkins School of Medicine, Baltimore, Maryland (Dr Handa, Dr Tagami, Dr Ebrahimi, Dr Janiak), and Department of Medicine, University of California at San Diego, La Jolla, California (Dr Leibundgut, DrWitztum, Dr Tsimikas).

from converting apo(a) to plasmin.[24] Unlike plasminogen, apo(a) is not widely distributed among different species and, instead, is uniquely present only in humans, nonhuman primates, and Old World monkeys. It should be noted that apo(a) is distinct from apoAI, the major protein moiety of high-density lipoproteins.

In humans, Lp(a) has been shown to have the unique property of binding OxPL and accounts for 85% or more of all PC-containing OxPL found on lipoproteins in plasma, as determined by the binding of murine monoclonal antibody E06.[25] It has been speculated that Lp(a) may become atherogenic because it has enhanced binding to arterial intimal proteoglycans, and thus increases local concentrations of proinflammatory OxPL. We thus sought to test the hypothesis that OSEs formed in the posterior pole, which is a high oxidative stress environment, are proinflammatory and toxic, resulting in retinal injury unless neutralized by a variety of mechanisms. In this study, we looked specifically at the role of OxPL in AMD as an OSE, and particularly those OxPL associated with Lp(a). To address this hypothesis, we have taken advantage of unique transgenic mice that express wild-type human Lp(a), which has the capacity to bind OxPL, and compared them to a different transgenic model that expresses a mutant form of apo(a), in which the Lp(a) lacks the ability to contain immunologically detectable OxPL, as detected by monoclonal antibody E06. We have studied the impact of accumulated OxPL in the fundus of these two transgenic mouse models of Lp(a).

METHODS

HUMAN TISSUE PROCESSING

The protocol in this study adhered to the tenets of the Declaration of Helsinki for research involving human tissue. Globes from 43- to 95-year-old donors were obtained from the National Development and Research Institutes, Inc, Philadelphia, Pennsylvania, within 6 hours of death, and when applicable, donors had been on life support for less than 24 hours (Table 1). Globes were selected for early AMD, which was defined by clinical history and the presence of basal deposits thicker than the normal height of an RPE cell (ie, >8 μm), as defined by Sarks using our previously described protocol.[26,27] Macular calottes were fixed for 1 hour in 2% paraformaldehyde with 20 mM butylated hydroxytoluene (BHT) and then cryoprotected by progressive infiltration in 10% and 20% sucrose in phosphate-buffered saline (PBS) (w/v) before freezing in 2:1 sucrose 20% (w/v):OCT compound at −80°C. We also assessed a second cohort of maculas by using autopsy eyes (n=9; Table 1) obtained from the Wilmer Eye Institute Pathology Division after approval from the Human Subjects Committee at Johns Hopkins University. Eyes were fixed in 4% formaldehyde, paraffin embedded, sectioned to 4 μm thickness, and deparaffinized with xylene and an ethanol gradient.

CELL CULTURE

The routine maintenance of the established, nonimmortalized human RPE cell line ARPE-19 has been previously described.[28] For experiments, ARPE-19 cells were seeded at 100,000/cm^2 in 6 well plates containing Dulbecco's Modified Eagle medium (DMEM)/F12 with 15 mM HEPES buffer and 10% fetal bovine serum (FBS) and 2 mM L-glutamine solution at 37°C for 1 week, and serum was withdrawn in DMEM/F12+1% bovine serum albumin (BSA) for 3 days to render ARPE-19 cells quiescent.

RNA EXTRACTION

Total RNA was extracted using the RNeasy Mini Kit (Qiagen Inc) according to the manufacturer's recommendation. RNA quality was confirmed with the Agilent Bioanalyzer (Agilent Technologies, Inc, Palo Alto, California).

TAQMAN RT-QPCR

Reverse transcription was performed using random hexamers and MultiScribe reverse transcriptase according to the manufacturer's recommendations (Applied Biosystems, Foster City, California). Quantitative real-time reverse transcription–polymerase chain reaction analysis (QRT-PCR) was performed using Assay-on-Demand primers and probe sets from Applied Biosystems with the ABI StepOnePlus Taqman system (Applied Biosystems). β-Actin was used for normalization. The unpaired *t* test was used to compare the differential gene expression between conditions.

WILD-TYPE LP(A) AND MUTANT LP(A) MICE

In this study we use two Lp(a) transgenic mouse models. Both Lp(a) models express human apo(a) and human apoB-100 to generate authentic Lp(a) particles, as human apo(a) does not covalently bind to murine apoB.[29-31] One Lp(a) model expresses a truncated human (a) variant, termed **WT Lp(a)**, of which the Lp(a) binds immunologically detectable OxPL by murine monoclonal antibody E06. The second Lp(a) transgenic model, termed **mutant LBS$^-$ Lp(a) mice**, expresses a similarly sized mutant apo(a) but with a defective lysine binding site (LBS) on kringle IV-10. Mutant apo(a) mice contain a defective KIV_{10} LBS in the KIV_{10} LBS of apo(a), which were generated using a cDNA construct where Asp^{55} and Asp^{57} residues in the KIV10 LBS were replaced with Ala^{55} and Ala^{57} residues, as reported.[30] This mutant Lp(a) does not have detectable OxPL by E06. These models were previously described in detail.[29] In both murine models, the apo(a) construct used to generate apo(a) transgenic mice contains the apoE promoter and 8 KIV units (KIV_1, a single copy of KIV_2, a fusion of KIV_3 and KIV_5, KIV_6 to KIV_{10}), KV, and the inactive protease-like domain, and were generated on a C57BL/6J×SJL background, as previously described.[31]

Lp(a) mice were generated by crossing hemizygous apo(a) mice with hemizygous mice expressing human apoB-100, which were previously generated with an apoB mutation in codon 2,153 that prevented apoB-48 synthesis.[32] Mutant LBS$^-$ apo(a)/Lp(a) mice were generated by crossing hemizygous mutant LBS$^-$ apo(a) mice with hemizygous human apoB-100 mice. Mice were housed in a barrier facility with a 12-hour light/12-hour dark cycle, and fed either a normal chow diet or a chow diet containing 1.25% cholesterol and

21% milk fat. Mice were genotyped by obtaining DNA from the tip of the tail and performing PCR using MyTaq HS Red Mix (Bioline, Inc, Taunton, Massachusetts). Forward and reverse primers for apo(a) were 5′-GACGGGAGACAGAGTGAAGC-3′ and 5′-TACCTAAACCACGCCAGGAC-3′, respectively, and for apoB-100 5′-GAAGAACTTCCGGAGAGTTGCAAT-3′ and 5′-CTCTTAGCCCCATTCAGCTCTGAC-3′, respectively. Mice were sacrificed at 12 months of age. All experiments were conducted according to the ARVO Statement for the Use of Animals in Ophthalmic and Vision Research, and the research was approved by the Institutional Research Board at the Johns Hopkins Medical Institutions.

TABLE 1. DEMOGRAPHICS OF DONOR EYES WITH AND WITHOUT AMD

DONOR	AGE (YEARS)	SEX	RACE	AMD (YES/NO)	D-E (HOURS)
Cohort 1					
1	74	F	C	Y	2.5
2	76	M	C	Y	4
3	76	F	C	Y	6.3
4	77	M	C	Y	3
5	84	M	C	Y	4.5
6	84	M	C	Y	6
7	85	F	C	Y	2.5
8	87	F	C	Y	3
9	87	F	C	Y	5.5
10	90	F	C	Y	4
11	90	M	C	Y	2.5
12	91	M	C	Y	2
13	91	F	C	Y	2.5
14	91	F	C	Y	5
15	93	F	C	Y	5.5
16	94	F	C	Y	5.5
17	95	F	C	Y	5
18	95	F	C	Y	3
19	43	M	C	N	6
20	46	M	C	N	4
21	67	M	C	N	5
22	70	F	C	N	6
23	76	M	C	N	3.5
24	78	F	C	N	4.5
25	80	F	C	N	6
26	95	F	C	N	3
Cohort 2					
1	55	M	C	Y	20
2	60	M	C	Y	28
3	83	F	C	Y	14
4	87	M	C	Y	24
5	91	M	C	Y	22
6	77	F	C	N	Unknown
7	84	M	C	N	44
8	84	F	C	N	75
9	95	F	C	N	Unknown

AMD, age-related macular degeneration; C, Caucasian; D-E, death to enucleation.

TISSUE PREPARATION

After mice were sacrificed and eyes were enucleated, one eye was fixed in 2.5% glutaraldehyde and 1% paraformaldehyde in 0.08M cacodylate buffer for transmission electron microscopy. The central 2×2-mm tissue temporal to the optic nerve was postfixed with 1% osmium tetroxide and dehydrated and embedded in Poly/Bed 812 resin (Polysciences, Inc, Warrington, Pennsylvania). Semithin sections were stained with toluidine blue. Ultrathin sections were stained with uranyl acetate and lead citrate. The contralateral eye was fixed in 2% paraformaldehyde with 20 mM BHT and cryopreserved, as described earlier, for immunohistochemical analysis.

ENZYME-LINKED IMMUNOSORBENT ASSAY FOR TOTAL APO(a), LP(a), OxPL/APO(a), AND OxPL/apoB IN MOUSE PLASMA

Both transgenic Lp(a) mice overexpress apo(a) in greater proportion to human apoB-100; therefore, they have circulating free apo(a), Lp(a) [apo(a) covalently bound to human apoB-100], and apo(a) noncovalently bound to mouse apoB, as previously described.[33,34] Therefore, "total apo(a)" and Lp(a) were both measured, as previously described.[33,34] The presence of total apo(a), Lp(a), OxPL/apoB-100, and OxPL/apo(a) in mouse plasma was determined by a variety of immunoassays, as previously described.[34,35] MB47 is an IgG murine monoclonal antibody that binds near the LDL-receptor binding domain of human apoB-100.[36] E06 is a murine monoclonal IgM natural antibody cloned from apoE$^{-/-}$ mice that binds the PC headgroup of PC containing OxPL, and recognizes OxPL whether free or covalently bound to proteins, but does *not* bind to unoxidized, native PC containing PL.[37,38] To determine total apo(a) levels in WT Lp(a) and mutant LBS^{-} Lp(a) mice, apo(a) was captured on microtiter well plates with LPA4 (5 μg/mL) and apo(a) detected with biotin-LPA4 (LPA4 binds to a TRNYCRNPDAEIRP epitope present on KIV-5, KIV-7, and KIV-8 of apo(a), and therefore the same antibody can be used in a sandwich ELISA). Lp(a) levels were measured in transgenic WT and mutant Lp(a) mice by immobilizing MB47 (5 μg/mL), a murine monoclonal antibody to human apoB-100 that does not cross-react with mouse apoB, on microtiter well plates for capture of human apoB-100; plasma was added (1:400), and Lp(a) detected with antibody LPA4. For OxPL/apoB sandwich ELISA, we used MB47 (5 μg/mL) as capture antibody, which was plated overnight, and then plasma (1:50 dilution) was added and OxPL detected with biotinylated E06 (2 μg/mL). For OxPL/apo(a) sandwich ELISA, LPA4 (5 μg/mL) was used as capture antibody; it was plated overnight and then plasma (1:50 dilution) was added and OxPL detected with biotinylated E06 (2 μg/mL). Values are reported as relative light units per 100 ms using chemiluminescent ELISA.

IMMUNOHISTOCHEMISTRY

A sheep polyclonal anti-"Lp(a)" biotinylated antibody (Abcam, Inc) and LPA4, which does not cross-react with plasminogen,[39] were used to detect apo(a). MB47 was used to detect human apoB-100[36] and E06 to detect OxPL. Antigens were retrieved with the Target Retrieval System (Dako, Inc, Carpinteria, California). Sections were incubated with blocking serum for 1 hour; with sheep polyclonal anti-Lp(a) biotinylated antibody (1:100), mouse anti-apo(a) monoclonal antibody (LPA4; 1:1000), anti-apoB-100 monoclonal antibody (MB47; 1:100), or anti-OxPL mouse monoclonal IgM (E06; 1:100), and equivalent concentrations of mouse IgG or IgM isotype controls overnight at 4°C; with biotinylated anti-mouse IgG (1:10,000; Vector Laboratories, Inc, Burlingame, California) or IgM (1:4000; Vector Laboratories) for 60 minutes; and then with ABC-AP (Vector Laboratories) for 30 minutes. The chromagen was developed with 5-bromo-4-chloro-3-indoyl phosphate (BCIP)/nitroblue tetrazolium (NBT) kit (Vector Laboratories) supplemented with levamisole. Sections were viewed with a light microscope equipped with the Cri-Nuance system (Caliper Life Sciences, Inc, Hopkinton, Massachusetts) to subtract out the melanin. Immunolabeling was assessed for tissue distribution within each section. Relative immunolabeling abundance was assessed by the extent of the labeling area. Staining intensity was a secondary criterion, but it was utilized only within the same tissue sections to exclude unintentional confounding influences across donors.

MOUSE IMMUNOFLUORESCENCE STUDIES

For fluorescence immunohistochemistry, mouse cryosections (8 μm) were first blocked with 2% donkey serum and avidin/biotin blocking reagent (Vector Laboratories), or treated with a mouse-on-mouse (MOM) blocking reagent for 1 hour at room temperature. Sections were then incubated with the primary antibody: rabbit polyclonal anti-annexin V (1:200, Abcam), rat monoclonal anti-C3 (1:100; Chemicon, Billerica, Massachusetts), rabbit polyclonal anti- C3d (1:100, Abcam), rabbit polyclonal anti-C5 (1:20, Abcam), rabbit polyclonal anti-C5b-9 (1:200, Abcam), sheep polyclonal anti-CFH (1:100, Abcam), goat polyclonal anti-Crry (1:50; Santa Cruz Biotechnology, Inc, Santa Cruz, California), mouse monoclonal anti-CD59 (IgG2b, 1:50, Abcam), rabbit polyclonal anti-rhodopsin (1:100, Abcam), rabbit polyclonal anti-HO-1 (1:200, Abcam), goat polyclonal anti-NQO1 (1:50, Santa Cruz Biotechnology), or mouse E06 IgM antibody to OxPL (1:100), overnight at 4°C, washed with PBS, and incubated with donkey anti-goat-Alexa fluor 647 (1:1000; Life Technologies, Grand Island, New York), donkey anti-goat-FITC (1:1000, Santa Cruz Biotechnology), donkey anti-sheep-Alexa488 (1:1000, Invitrogen), donkey anti-rat-Alexa488 (1:1000, Invitrogen), goat anti-mouse IgM-Alexa594 (1:2000, Invitrogen), goat anti-mouse IgGb2-Alexa fluor 594 (1:500, Invitrogen), goat anti-rabbit-FITC (1:1000, Santa Cruz Biotechnology), or a MOM biotinylated anti-mouse IgG secondary antibody, followed by rhodamine avidin D (Vector Laboratories). Appropriate mouse, goat, or rabbit IgG (Santa Cruz Biotechnology) were used as isotype controls. Z-stack images of tissue sections were imaged using a Zeiss ZEN LSM 710 confocal microscope.

ELECTRON MICROSCOPY

Ultrathin sections were examined with a JEM-100 CX electron microscope (JEOL, Ltd, Tokyo, Japan) in the Wilmer Core Facility. RPE, Bruch's membrane, and choriocapillaris ultrastructural changes were graded for severity. Each change was graded on an ordinal

scale from 0 to 3 using a minimum of 50 sections by a masked observer. Ordinal logistic regression analysis was performed using Stata Version 8 (Statacorp, College Station, Texas), as previously described.[40-42]

TUNEL ASSAY

Cryosections were dried at room temperature for 30 minutes. After rinsing the sections with PBS, tissue was permeabilized with 0.1% triton X-100 and 0.1% sodium citrate for 2 minutes on ice. TUNEL labeling was performed with an In Situ Cell Death Detection Kit, TMR red (Roche Diagnostics, GmbH, Mannheim, Germany). Sections were incubated and covered with parafilm for 60 minutes at 37°C. Sections were counterstained with DAPI (Vector Laboratories). Positive controls were created by incubating tissue with 1 mg/mL DNase I in 50 mM Tris-HCl, pH 7.5, 1 mM magnesium chloride, and 1 mg/mL BSA for 10 minutes at room temperature. TMR and DAPI were visualized with a confocal microscope (Zeiss 510 META confocal microscope; Carl Zeiss MicroImaging, Inc, Thornwood, New York) at 543 nm and 455 nm, respectively.

RESULTS

OxPL ACCUMULATE IN BRUCH'S MEMBRANE

Utilizing monoclonal antibody E06, we first determined whether PC-containing OxPL were found in the human macula. We evaluated 18 AMD specimens and 8 controls ranging in age from 43 to 95 years (Table 1). We found that OxPL accumulate in Bruch's membrane and choroid of all the control (n=8) and AMD maculas (n=18; Figure 1). The distribution was very similar between AMD and control samples. However, OxPL labeling was also detected in drusen deposits of all AMD samples (Figure 1).

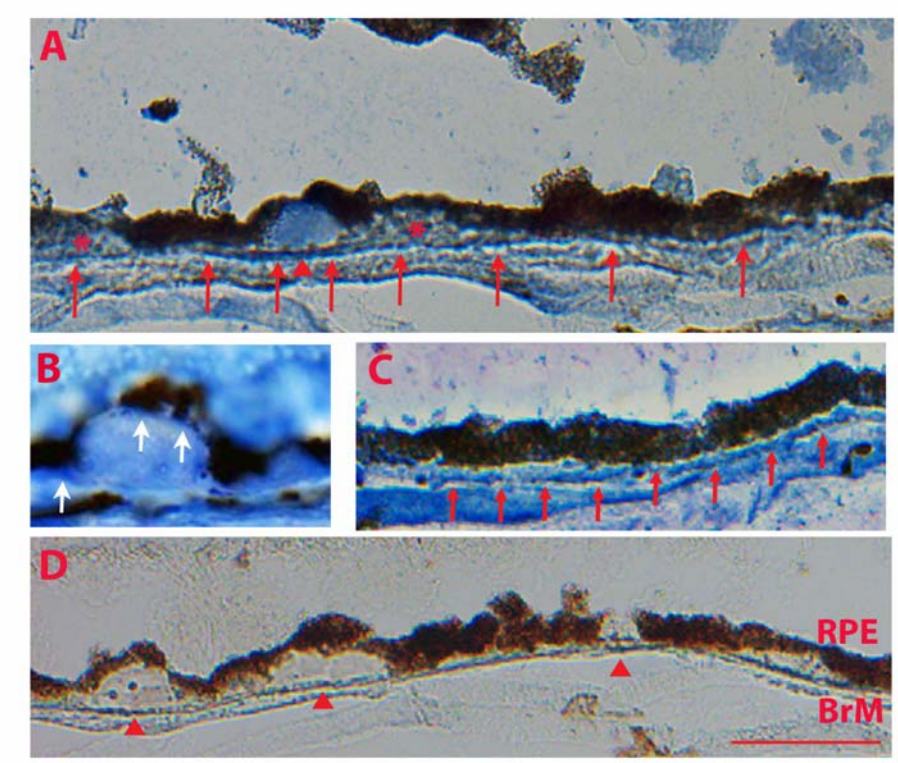

FIGURE 1

OxPL immunolabeling using E06 antibody of human maculas. A, Macula of a 76-year-old woman with early age-related macular degeneration (AMD). Bruch's membrane (BrM), especially the choriocapillaris (CC) basement membrane (red arrows), and the choroid show immunostaining for OxPL. A druse (red arrowhead) adjacent to basal laminar deposits (*) is prominently stained. The retinal pigment epithelium (RPE) does not stain. B, Higher-power view of a druse from an 84-year-old man with early AMD. Note the punctate-like staining pattern, and staining within BrM along the RPE basement membrane (white arrows). C, OxPL staining is seen in a 76-year-old woman without AMD. The CC basement membrane (red arrows) and choroid are most prominently stained for OxPL. D, IgM control shows no immunolabeling. Red arrowheads point to drusen. Bar=50 μm.

APO(a) LOCALIZES TO OUTER BRUCH'S MEMBRANE IN AMD

We next determined the extent that apo(a) accumulates in the macula. Using a commercially available anti-"Lp(a)" antibody, immunolabeling for Lp(a) was seen within the choroid and outer Bruch's membrane, with the strongest labeling within the choriocapillaris basement membrane in both AMD (Figure 2A) and non-AMD (Figure 2B) maculas. While the RPE did not stain in any samples, punctate apo(a) labeling is observed within drusen and basal deposits, another histopathological marker for AMD, in 5 of the 18 AMD samples (Figure 2A). A limited number of our samples (n=3) contained neuroretina. Immunostaining in these samples for apo(a) was confined to the retinal vasculature (Figure 2D).

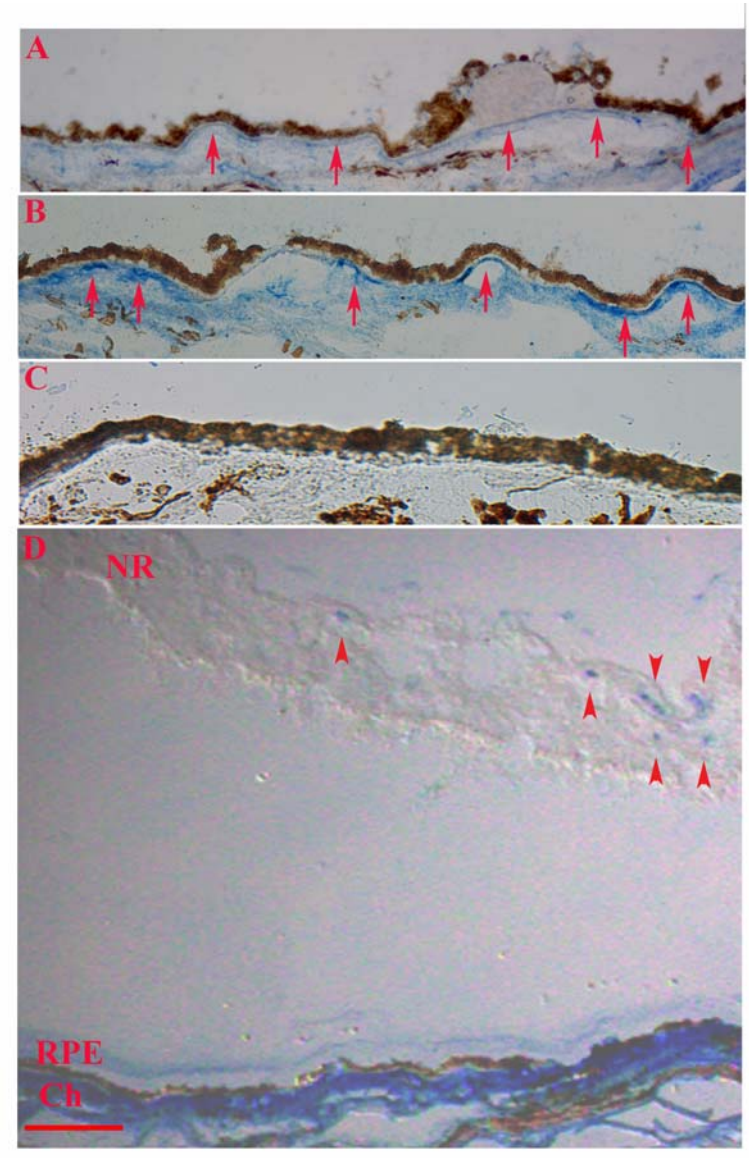

FIGURE 2

Apo(a) immunolabeling of human maculas. A, A 74-year-old woman with early age-related macular degeneration (AMD). Outer Bruch's membrane, especially the choriocapillaris basement membrane (red arrows), and the choroid show immunostaining for apo(a). While the retinal pigment epithelium (RPE) does not label for apo(a), a large druse (150 μm) shows punctate and vacuole-like immunolabeling. B, A 70-year-old woman without AMD. Immunolabeling for apo(a) is seen in outer Bruch's membrane, including the choriocapillaris basement membrane (red arrows) and the choroid (Ch). C, IgG isotype control showing no labeling. D, An 80-year-old woman without AMD. Immunostaining for apo(a) is seen within retinal vasculature (red arrowheads), but not the neurosensory retina (NR) itself. Bar=150 μm.

According to the manufacturer, this commercially available antibody was purified using a human plasminogen-Sepharose affinity column to remove cross-reactivity to plasminogen, followed by an apo(a)-Sepharose affinity column. To fully remove doubt of potential plasminogen cross-reactivity, we looked at a different cohort (n=5 AMD, n=4 age-matched controls) using the monoclonal antibody LPA4, which does not bind plasminogen, and found a similar labeling pattern. Immunolabeling for apo(a) was consistent and diffuse in the choroid of all AMD (n=5) and age-matched control (n=4) maculas. In control samples, minimal if any apo(a) immunolabeling was seen in the RPE or Bruch's membrane. In the AMD samples, subtle immunostaining was seen in the basal RPE or within Bruch's membrane compared to the choroid. However, the choriocapillaris basement membrane of Bruch's membrane had relatively more intense staining in 3 of the 5 AMD samples compared to what was seen in the choriocapillaris basement membrane,

compared to the rest of Bruch's membrane, in controls. Drusen and basal deposits were immunostained with mild intensity compared to that seen in the choroid (Figure 3).

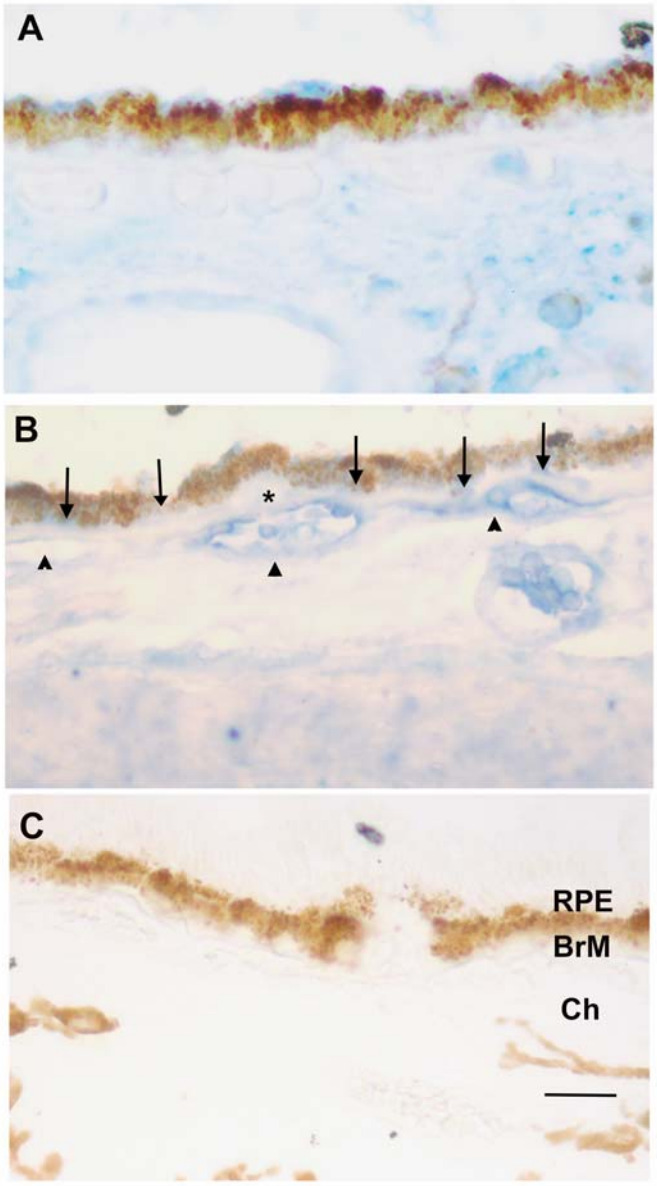

FIGURE 3

Apo(a) immunolabeling of human maculas using anti-LPA4, an apo(a) specific monoclonal antibody. A, An 84-year-old man without age-related macular degeneration (AMD) shows punctate and diffuse labeling for apo(a) throughout the choroid (Ch), but labeling is minimal to absent in Bruch's membrane (BrM). Extracellular debris at the apical surface of the retinal pigment epithelium (RPE) stains for apo(a). B, A 91-year-old man with early AMD shows diffuse apo(a) labeling throughout the choroid, especially in the choriocapillaris (arrowheads), with light staining as well in Bruch's membrane (BrM) (arrows). A small druse (*) stains lightly for apo(a). C, IgG control from the same 91-year-old man without labeling. Bar=25 μm.

We next evaluated the distribution of apoB-100 in cohort 2 using MB47, which binds to apoB-100 near the LDL-receptor binding domain, and binds to apoB on OxLDL even with extensive oxidation. In controls and nondiseased regions of AMD samples, apoB-100 immunolabeling was occasionally observed in RPE cells and occasionally in Bruch's membrane. Staining in the choroid was mosaic in distribution compared with apo(a), which was widely distributed. While not all basal deposits and drusen of AMD samples stained, others displayed obvious apoB-100 punctate labeling. ApoB-100 staining in the choroid was light in intensity compared to regions of drusen or staining within the RPE (Figure 4). In Figure 5, photomicrographs of the macula from a 55-year-old man with AMD show staining for apo(a) and apoB-100 at the base of the RPE overlying a druse and within outer BrM.

The distribution of apo(a) near blood vessels suggests a systemic origin, with delivery of Lp(a) to the macula from either the retinal or choroidal circulation. However, apo(a) could be locally produced because the RPE can manufacture apoB-100 lipoprotein particles, but it is unknown if they can synthesize apo(a). Apo(a) is only known to be primarily synthesized in hepatocytes. To determine if the RPE could express apo(a), we treated human ARPE-19 cells with IL-6 at 1 to 10 ng/mL, or with tumor necrosis factor (TNF)-α at 0 to 200 ng/mL, two known stimulators of apo(a).[43] We did not find measurable apo(a) transcript levels, in contrast to robust levels of apo(a) from hepG2 cells using RT-qPCR (data not shown). These results suggest that RPE cells are not likely making apo(a) in vivo, although further work, such as verifying the lack of expression in primary RPE cell lines or using a model that can express drusen proteins,[44] is necessary to definitely exclude that the RPE can express apo(a).

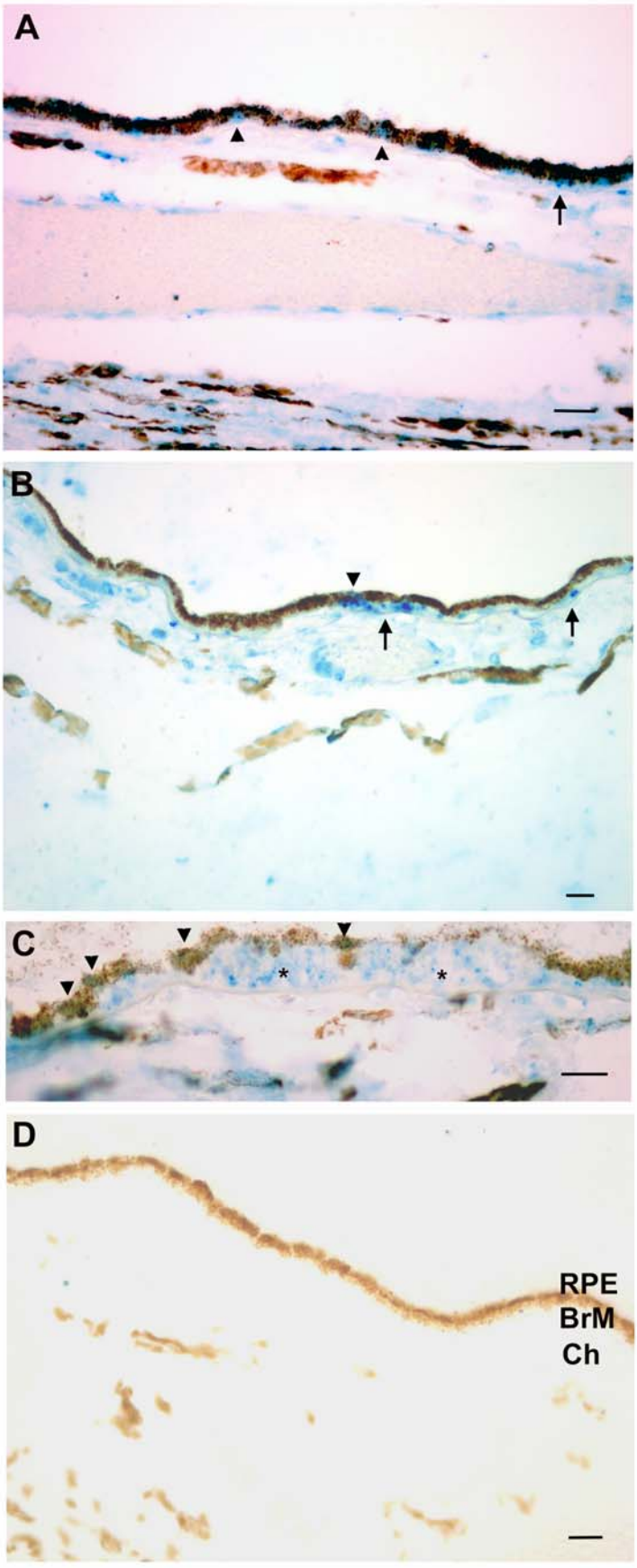

FIGURE 4

ApoB immunolabeling of human maculas using MB47, which binds apoB-100. A, A 77-year-old woman without age-related macular degeneration (AMD) shows mosaic immunolabeling for apoB in the choroid (Ch) and Bruch's membrane (BrM) (arrow). There is minimal labeling in the retinal pigment epithelium (RPE) (arrowheads). B, A 91-year-old man with AMD shows mosaic immunolabeling for apoB in the choroid, punctate staining in basal deposits (arrows) within Bruch's membrane, and staining of the RPE (arrowhead). C, An 83-year-old woman with AMD shows obvious punctate immunolabeling in a large druse (*), with mosaic labeling in the choroid. Some RPE are labeled for apoB (arrowheads). D, IgG control from the same 83-year-old woman. Bar=25 μm.

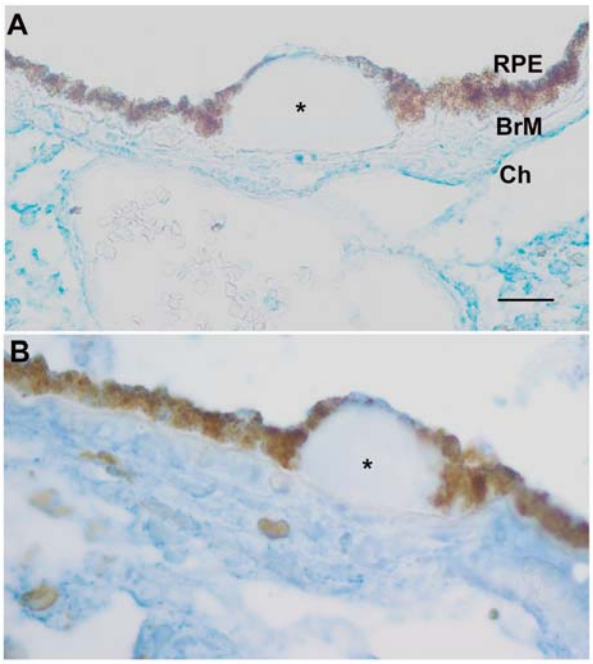

FIGURE 5

Immunolabeling for apo(a) and apoB-100 in a 55-year-old man with age-related macular degeneration. A, Immunolabeling for apoB in the choroid (Ch) and at the apex of the same druse (*). B, Obvious apo(a) labeling is diffusely distributed in the choroid, at the apex of the druse (*), and within remnants of retinal pigment epithelium (RPE) cells overlying the druse. BrM, Bruch's membrane. Bar=25 μm.

MUTANT LBS⁻ LP(a) MICE SHOW PHENOTYPIC FEATURES OF AMD

We have shown that Lp(a) binds OxPL in human plasma. With evidence of apo(a) in Bruch's membrane/choroid and OxPL in human maculas, we next addressed the hypothesis that apo(a) will bind OxPLs that form in the fundus and prevent an inflammatory-mediated pathologic phenotype by evaluating transgenic WT Lp(a) and mutant LBS⁻ Lp(a) mice. Mice were fed either a normal chow or a high-fat diet from 2 to 12 months of age and then sacrificed. Plasma was obtained after 36 weeks to assess the levels of total apo(a), Lp(a), OxPL/apo(a), and OxPL/apoB. Compared to WT Lp(a) mice, mutant LBS⁻ Lp(a) mice had higher (~2×) total apo(a) and Lp(a) plasma levels, but much lower OxPL/apoB (10×) and OxPL/apo(a) (5×) levels, as shown in Figure 6.

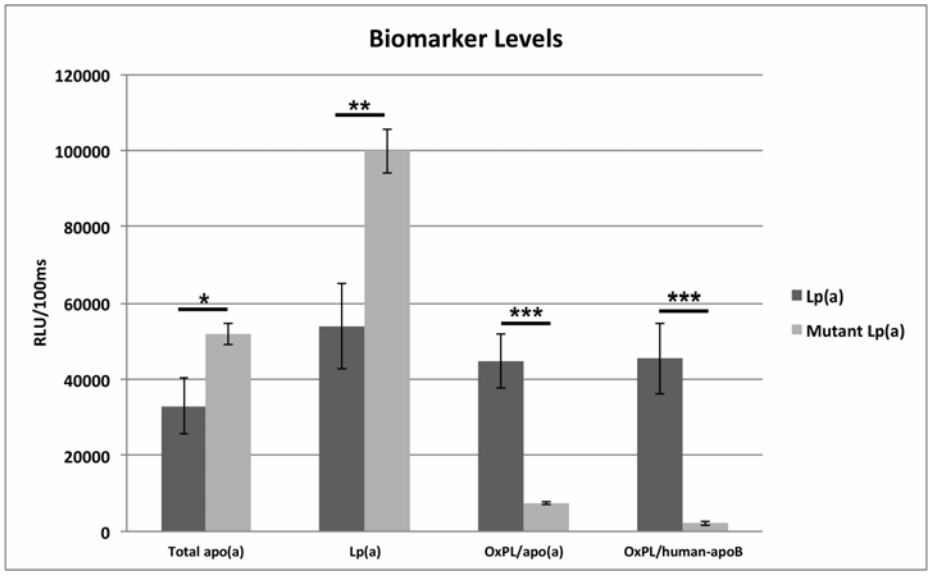

FIGURE 6

Biomarkers in the serum of Lp(a) mouse models after 36 weeks of high-fat diet. Bars indicate mean value and standard error of the mean. RLU, relative light units. **P*<.05; ***P*<.01; ****P*<.001.

We next evaluated the retinal morphology of these mice. WT Lp(a) and mutant LBS$^-$ Lp(a) mice that were fed a normal chow diet did not show significant morphologic changes on semithin sections (Figure 7, A and B). Twelve-month-old WT Lp(a) mice (n=10) fed a high-fat diet had minimal morphologic changes to the photoreceptors, RPE, Bruch's membrane, and choroid that are compatible with aging (Figure 7C). In contrast, mutant LBS$^-$ Lp(a) mice on a high-fat diet (n=10) had dysmorphic RPE with prominent vacuoles in 10 of 10 mice examined (Figure 7D). Drusen, a hallmark sign of AMD, were present in 4 of 10 mutant LBS$^-$ Lp(a) mice examined (Figure 7E), whereas only one druse was observed in a single WT Lp(a) mouse.

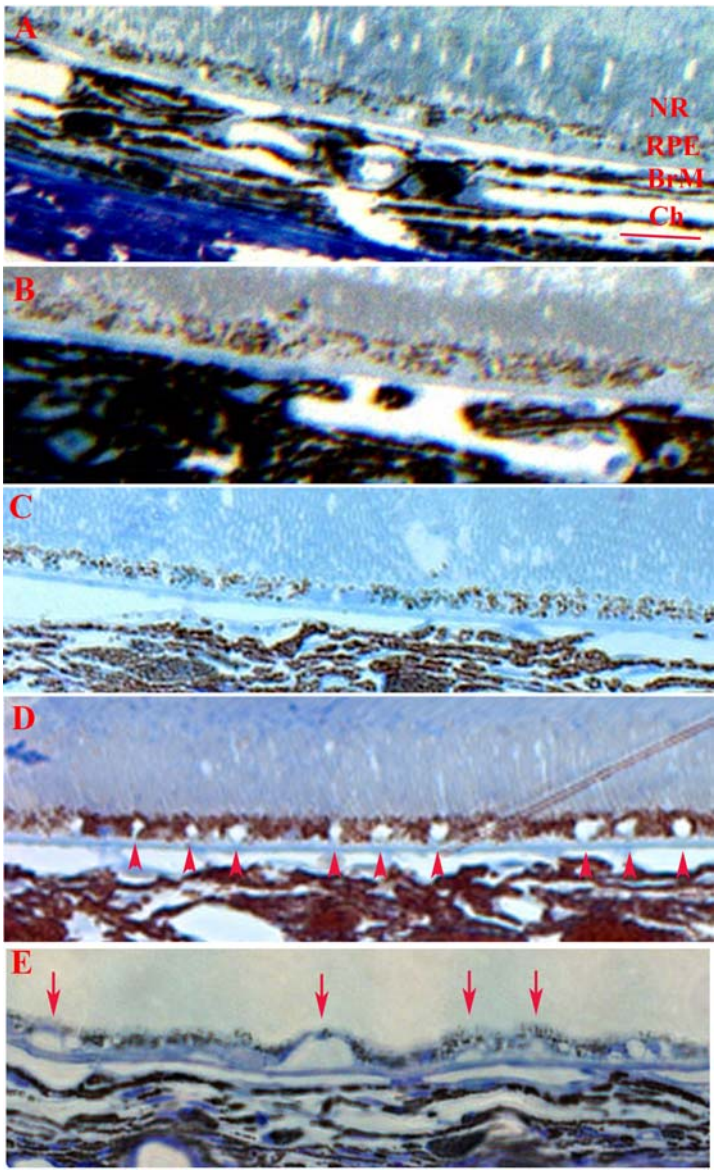

FIGURE 7

Semithin sections of WT Lp(a) and mutant LBS$^-$ Lp(a) mouse fundi. A, A 12-month-old WT mouse given a normal chow diet shows normal morphology of the retina, retinal pigment epithelium (RPE), Bruch's membrane (BrM), and choroid (Ch). B, A 12-month-old mutant Lp(a) mouse given a normal chow diet shows normal fundus morphology compared to WT mice. C, A 12-month-old WT Lp(a) mouse on a high-fat diet (HFD) also had normal fundus morphology. D, A 12-month-old mutant LBS$^-$ Lp(a) mouse on a HFD with morphologically normal photoreceptor outer segments and prominent vacuoles with the RPE (arrowheads). E, A 12-month-old mutant LBS$^-$ Lp(a) mouse on a HFD with drusen (arrows) and thinned RPE overlying drusen. NR, neurosensory retina. Bar=25 μm.

We then evaluated the ultrastructural features of the retinas of both WT and mutant Lp(a) mice after normal chow and a high-fat diet. WT Lp(a) and mutant LBS$^-$ Lp(a) mice on normal chow did not exhibit ultrastructural changes in electron micrographs (Figure 8, A and B). On the other hand, we observed marked differences in ultrastructure between WT and mutant Lp(a) mice on the high-fat diet. Loss of basal infoldings, a marker of epithelial injury,[45-47] and cytoplasmic vacuoles, which have been identified in RPE that overlie drusen deposits,[48] are two relevant ultrastructural markers for RPE degeneration. While mild RPE and Bruch's membrane changes that are compatible with aging were observed in the WT mice (n=10) fed a high-fat diet, marked RPE and Bruch's membrane changes were observed in the RPE of mutant LBS$^-$ Lp(a) mice fed a high-fat diet. Figure 9, A through D, shows ultrastructure from retinas of WT Lp(a) mice with RPE cells that maintain their basal infoldings and have an occasional vacuole. These changes are typical of aging mice. In contrast, the RPE of mutant LBS$^-$ Lp(a) mice displayed marked ultrastructural abnormalities, including unprocessed photoreceptor tips at the basal portion of the cell, large membranous vacuoles, markedly dysmorphic mitochondria, and fewer, dilated basal infoldings, some of which were contiguous with large membranous vacuoles (Figure 9, E through H).

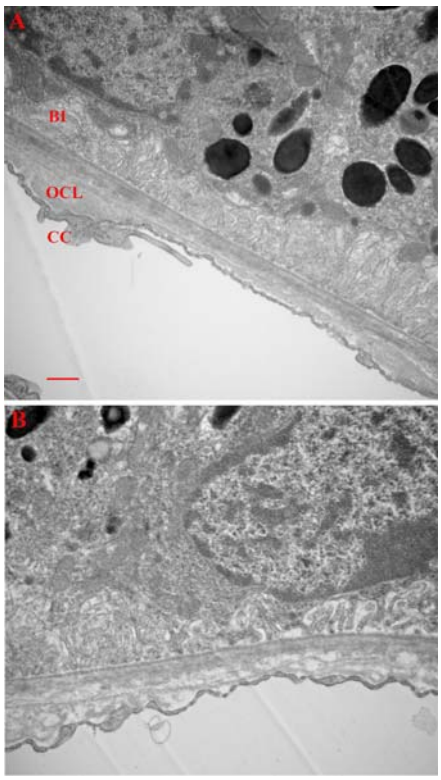

FIGURE 8

Electron microscopy of WT and mutant LBS$^-$ Lp(a) mice fed a normal chow diet. A, A 12-month-old WT Lp(a) mouse has ultrastructurally normal retinal pigment epithelium (RPE) with preserved basolateral infoldings (BI), melanin pigment, and mitochondria. Bruch's membrane has a small outer collagenous layer deposit (OCL), which is a normal aging change. The choriocapillaris (CC) has normal-appearing fenestrations. B, 12-month-old mutant LBS$^-$ Lp(a) mouse fed a normal chow diet also has ultrastructurally normal RPE, Bruch's membrane, and choriocapillaris. Bar=500 nm.

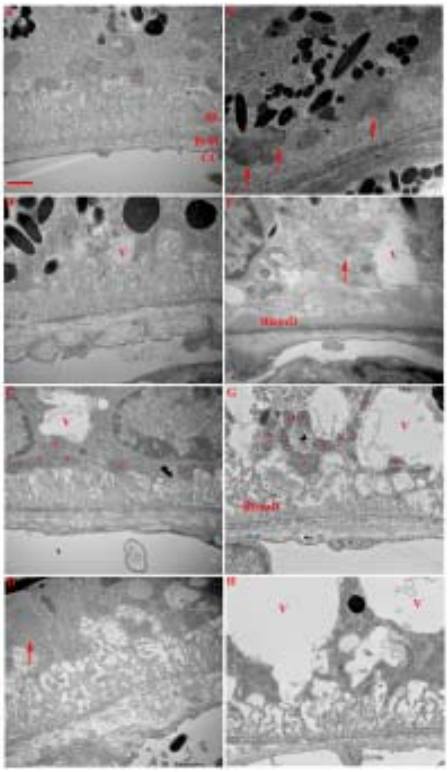

FIGURE 9

Electron microscopy of the retinal pigment epithelium (RPE) from WT and mutant LBS$^-$ Lp(a) mice fed a high-fat diet. A, A 12-month-old WT Lp(a) mouse has normal ultrastructural features of the RPE including basolateral infoldings (BI) and mitochondria (*). Bruch's membrane (BrM) has a regular structure without deposits, and the choriocapillaris (CC) has preserved fenestrations. B, In another WT Lp(a) mouse, the RPE contains membranous vacuoles but has preserved basolateral infoldings. BrM shows thickening of the outer collagenous layer, a normal aging change. The CC is preserved. C, Higher-power view of WT Lp(a) retinas showing a membranous vacuole, preserved BI, and mitochondria (*). D, WT Lp(a) mouse retinas showing some enlarged and fewer BI and undigested photoreceptor outer segments (POS; arrow), suggesting some RPE degeneration. E, 12-month-old mutant LBS$^-$ Lp(a) retinas with shortened, fewer BI and numerous unprocessed POS (arrows). F, Another mutant LBS$^-$ Lp(a) retina with large vacuole (V), large, bizarre unprocessed POS, and prominent heterogeneous basal laminar deposit (BlamD) between the RPE and RPE basement membrane. G, Another mutant mouse with RPE that had large vacuoles (V), few and dilated BI, abnormal internal structure of mitochondria (*), and prominent BlamD. The choriocapillaris endothelial fenestrations are preserved. H, Another mutant retina with marked vacuolization of the RPE and enlarged, fewer BI. Bar=500 nm.

Figure 10 illustrates the difference in Bruch's membrane changes between high-fat-diet-fed WT and mutant mice. WT Lp(a) mice fed a high-fat diet maintained normal Bruch's membrane architecture (Figure 10, A through C) with occasional mild thickening of Bruch's membrane due to outer collagenous layer deposits, an aging change that is not specific for AMD[49] (Figure 10C). In contrast, in the mutant mice, basal laminar deposits, which accumulate between the RPE cell and RPE basement membrane, were prominent with heterogeneous content, an ultrastructural feature associated with AMD[50] (Figure 10, D and E). Drusen were also confirmed by transmission electron microscopy (Figure 10F). Choroidal neovascular membranes were not observed in any specimens. Using semiquantitative regression analysis, we found that phenotypic changes between WT and mutant Lp(a) mice maintained on a normal diet were not different, but were distinct between the two models on the high-fat diet (Table 2). The phenotypic features of high-fat-diet-fed WT and mutant Lp(a) mice were compared using ordinal regression analysis. Mutant LBS$^-$ Lp(a) mice were at increased odds for developing more severe ultrastructural changes than WT Lp(a) mice, including RPE basolateral infolding changes (odds ratio [OR] 2.04, P<.001), RPE vacuoles (OR 5.10, P<.001), basal laminar deposits (OR 5.00, P<.001), outer collagenous layer deposits (OR 3.03, P<.001), but not choriocapillaris changes (OR 1.04, P=.70).

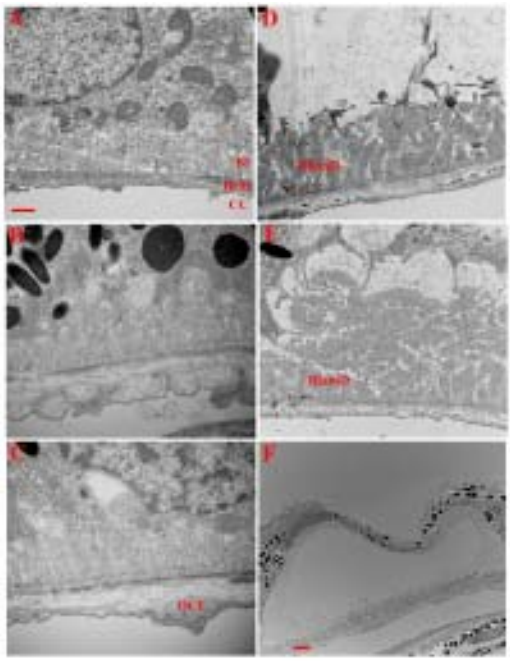

FIGURE 10

Electron microscopy of Bruch's membrane (BrM) from WT and mutant LBS$^-$ Lp(a) mice fed a high-fat diet. A, A 12-month-old WT Lp(a) mouse retina with normal-appearing retinal pigment epithelium (RPE) and BrM. B, WT Lp(a) mouse with mild thickening of the outer collagenous layer (OCL), a normal aging change. C, WT Lp(a) mouse with mild OCL deposit, a normal aging change. D, A 12-month-old mutant LBS$^-$ Lp(a) mouse retina with marked vacuolization of the RPE and prominent heterogenous basal laminar deposit (BlamD). E, Similar BlamD in retina of a different mutant mouse. F, Druse from a mutant LBS$^-$ Lp(a) mouse. BI, basolateral infoldings; CC, choriocapillaris. Bar=500 nm.

TABLE 2. REGRESSION ANALYSIS OF ULTRASTRUCTURAL CHANGES TO THE RETINAL PIGMENT EPITHELIUM, BRUCH'S MEMBRANE, AND CHORIOCAPILLARIS OF LP(a) AND MUTANT LP(a) MICE

	PERCENTAGE			
SEVERITY RATING	NORMAL DIET		HIGH-FAT DIET	
	Lp(a)	MUTANT Lp(a)	Lp(a)	MUTANT Lp(a)
Retinal pigment epithelial vacuole				
0	78.1	70.6	32.6	7.6
1	19.9	11.8	34.8	14.2
2	2.0	8.1	22.6	39
3	0	9.6	10	39.2
Retinal pigment epithelial infoldings				
0	94.7	76.1	10.6	2.2
1	3.97	7.2	37.4	32.4
2	0.66	2.2	28	25
3	0.66	14.5	24	40.4

TABLE 2. CONTINUED

SEVERITY RATING	PERCENTAGE			
	NORMAL DIET		HIGH-FAT DIET	
	Lp(a)	MUTANT Lp(a)	Lp(a)	MUTANT Lp(a)
Basal laminar deposit				
0	98.6	86.4	78.6	44.6
1	1.3	2.1	11.6	15.2
2	0	0	7.4	20.4
3	0	11.4	2.4	19.8
Outer collagenous layer deposit				
0	86.1	59.9	42.4	21.2
1	12.6	19.7	37.6	34.6
2	1.32	10.6	14	22.2
3	0	9.9	6	22
Choriocapillaris				
0	74.1	59.4	15.4	10.6
1	13.3	22.6	33.4	38
2	10.4	17.3	24	26.4
3	2.2	0.7	27.2	25

LBS$^-$ APO(a)/LP(a) MICE ACCUMULATE OxPL IN THE FUNDUS

Since mice fed chow did not exhibit phenotypic features of AMD, we focused the remaining studies on mice fed a high-fat diet to identify factors that could contribute to this phenotype. In WT mice (n=5), light staining for OxPL was seen throughout the retina, RPE, Bruch's membrane, and choroid (Figure 11, A and B). In contrast, mutant LBS$^-$ Lp(a) mice (n=5) accumulated more OxPL throughout all layers of the fundus than WT mice, as shown in Figure 11, C and D. OxPL labeling was more intense at the ellipsoid layer relative to other aspects of the photoreceptors in mutant mice (Figure 12A). Interestingly, staining with E06 highlighted the loss of the ellipsoid layer in mutant LBS$^-$ Lp(a) mice, a finding that has been associated with vision loss in AMD[51] (Figure 12B).

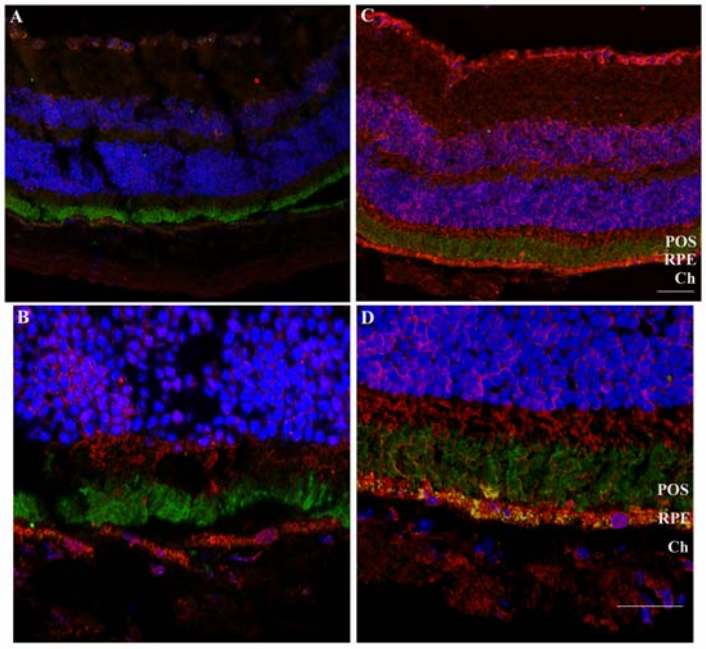

FIGURE 11

Fluorescence immunohistochemistry showing OxPL is more prominent in the retinas of mutant LBS$^-$ Lp(a) than WT Lp(a) mice fed a high-fat diet. A, A 12-month-old WT Lp(a) mouse shows minimal immunolabeling for OxPL using the E06 antibody (red). When present, labeling appears in inner layers and the retinal pigment epithelium (RPE). B, Higher magnification of panel A showing immunolabeling for OxPL in the outer nuclear layer of the retina and RPE. C, 12-month-old mutant LBS$^-$ Lp(a) mouse with strong immunolabeling for OxPL throughout all layers of the retina, RPE, Bruch's membrane, and choroid (Ch). D, Higher magnification of panel C showing strong OxPL labeling in the outer nuclear layer, photoreceptors, RPE, and choroid. POS, photoreceptor outer segment. (Blue, DAPI; Green, rhodopsin) Bar=25 μm.

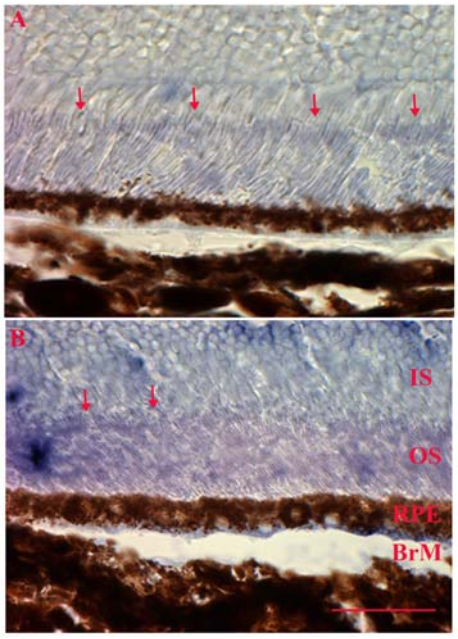

FIGURE 12

OxPL immunohistochemistry of the ellipsoid layer of photoreceptors. A, A 12-month-old WT Lp(a) mouse with immunolabeling for OxPL in the photoreceptors. The ellipsoid layer (arrows) is preserved. B, A 12-month-old mutant LBS$^-$ Lp(a) mouse with labeling for OxPL in the photoreceptors. The ellipsoid layer (arrows) is discontinuous. Note more obvious immunolabeling of Bruch's membrane (BrM) in the mutant compared to WT Lp(a) retina in panel A. IS, inner photoreceptors; OS, outer photoreceptor segments; RPE, retinal pigment epithelium. Bar=25 μm.

MUTANT LP(a) MICE HAVE REDUCED ANTIOXIDANT IMMUNOLABELING

We next evaluated the antioxidant response in the fundus of WT and mutant Lp(a) mice. NQO-1 immunolabeling was seen in the outer sensory retina, mainly in the photoreceptors, of both WT and mutant mice (Figure 13, A and C). NQO-1 labeling was also seen in the RPE of WT but not mutant Lp(a) mice. A speckled NQO-1 labeling pattern was observed in the choroid, which was more prominent in WT mice compared to mutants. HO-1 immunolabeling, like NQO-1, was more prominent in WT mice than in the mutants (Figure 13, B and D). In the neurosensory retina, HO-1 labeling was localized to the outer retina, with a similar staining pattern between WT and mutant mice, and also was evenly distributed in the RPE, again appearing similar between WT and mutant mice. A speckled HO-1 labeling pattern seen in the choroid of WT mice was more prominent than in mutant mice. These results indicate a reduced antioxidant abundance in mutant LBS$^-$ Lp(a) mice despite (or as a consequence of) abundant OxPL.

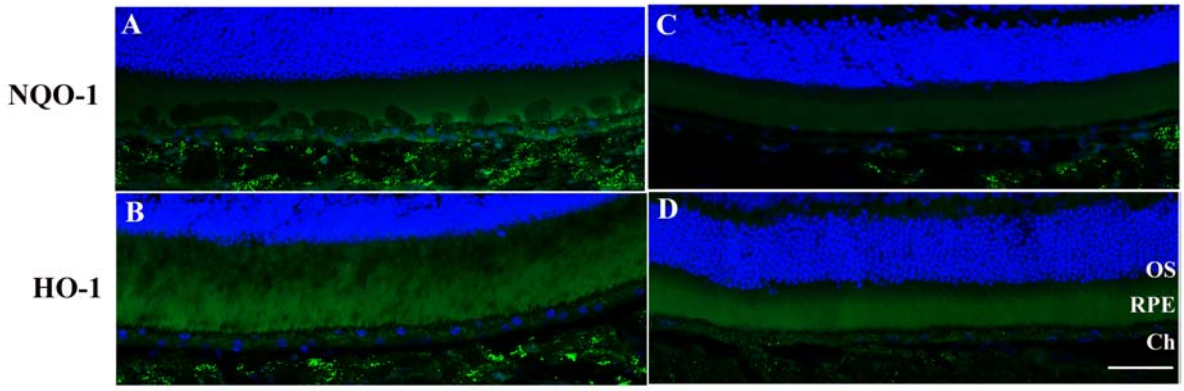

FIGURE 13

Fluorescence immunohistochemistry of antioxidant response in retinas of WT and mutant LBS$^-$ Lp(a) mice fed a high-fat diet. A, A 12-month-old WT Lp(a) mouse retina with immunolabeling for NQO-1 (green) in the outer photoreceptors (OS), retinal pigment epithelium (RPE), and choroid (Ch). B, Same WT Lp(a) retina with immunolabeling for HO-1 (green) in the outer photoreceptors, RPE, and choroid. C, A 12-month-old retina from mutant LBS$^-$ Lp(a) mouse with immunolabeling for NQO-1 confined to the choroid. D, Same retina from mutant mouse with minimal immunolabeling for HO-1 in the outer photoreceptors and choroid. (Blue, DAPI) Bar=25 μm.

MUTANT LP(a) MICE EXHIBIT INCREASED COMPLEMENT AND REDUCED COMPLEMENT REGULATOR IMMUNOSTAINING

Oxidative stress can magnify the innate immune response.[52] Because of the constellation of polymorphisms in genes associated with the complement pathway,[53-60] complement dysregulation is well recognized as an important arm of innate immunity in AMD. Compared to WT Lp(a) mice, mutant LBS$^-$ Lp(a) mice showed increased complement component labeling (Figure 14). In high-fat-diet-fed WT Lp(a) mice, C3 labeling in the neurosensory retina was weak, including the photoreceptors and choroid, but was prominent in RPE/Bruch's membrane (Figure 14A). In mutant Lp(a) mice, C3 immunolabeling was, for the most part, evenly distributed throughout all retinal layers, particularly strong in the inner relative to the outer photoreceptor segments and RPE/Bruch's membrane, and relatively weaker in the choroid (Figure 14B). C3d is the final degradation product of complement C3 and serves as a marker of C3 activation. Figure 14, C and D, shows strong C3d immunolabeling in mutant LBS$^-$ Lp(a) fundi compared to WT Lp(a) fundi. In particular, C3d labeling was more intense in the choroid, RPE, and ganglion cell layer than in other layers of the neurosensory retina.

Complement regulators of C3 showed the opposite immunolabeling pattern from complement components. Complement factor H (CFH) is a fluid phase regulator of C3. CFH immunolabeling in mutant LBS$^-$ Lp(a) mice was barely detectable compared to the more obvious labeling seen throughout all layers of the retina, RPE, Bruch's membrane, and choroid in WT Lp(a) mice (Figure 14, E and F). Crry is a cell membrane protein that is the main cell membrane regulator of C3 in the mouse. Crry immunolabeling was similar between WT and mutant mice (Figure 14, G and H). The Crry labeling was most intense in the photoreceptors and RPE compared to other regions of the retina and choroid.

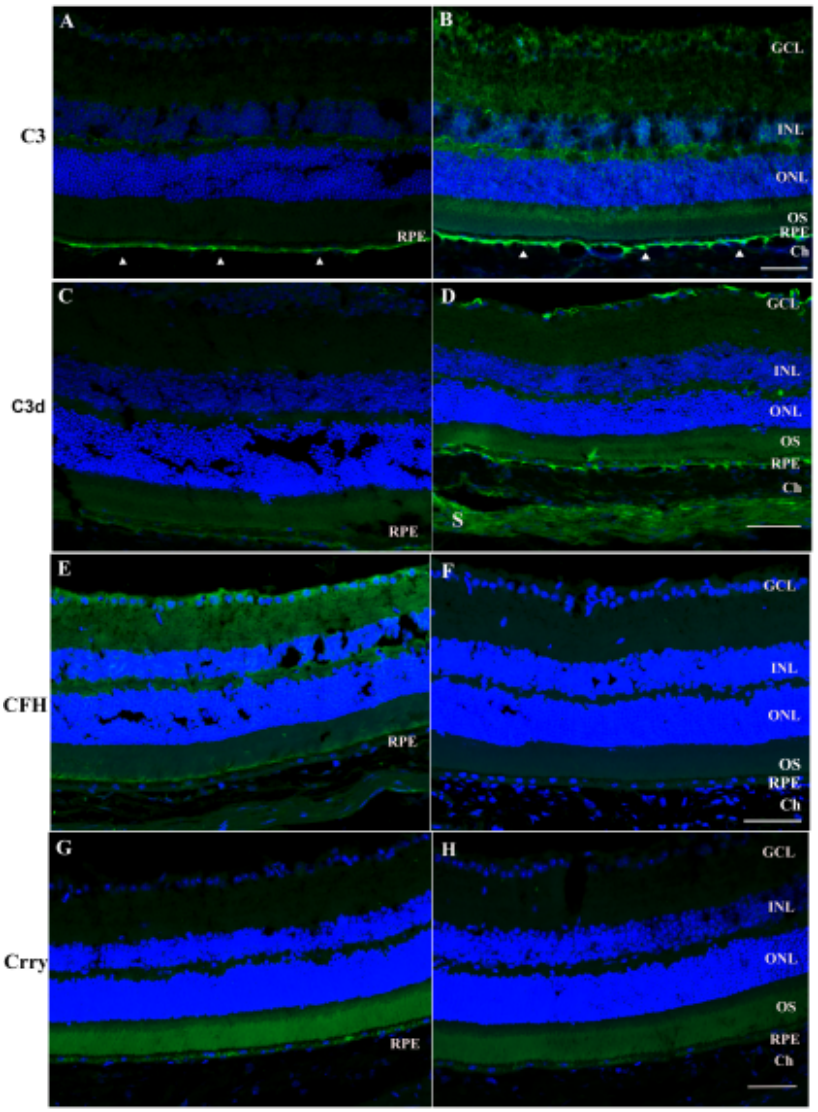

FIGURE 14

Fluorescence immunohistochemistry of C3 and its regulators in retinas of WT and mutant LBS$^-$ Lp(a) mice fed a high-fat diet. A, A 12-month-old WT Lp(a) mouse retina with immunolabeling for C3 (green) confined to the retinal pigment epithelium (RPE)/Bruch's membrane (BrM) junction (arrowheads). B, Retina from 12-month-old mutant LBS$^-$ Lp(a) mouse with strong C3 labeling throughout the retina, RPE/BrM junction (arrowheads). C, WT Lp(a) mouse retina with minimal C3d labeling in the fundus. D, Retina of mutant mouse has prominent labeling throughout the retina, RPE/BrM junction. E, WT Lp(a) retina with complement factor H (CFH) immunolabeling throughout the retina and RPE. F, Mutant retina with minimal CFH immunolabeling. G, WT Lp(a) retina with Crry immunolabeling mainly in the photoreceptors and RPE. H, Mutant retina with mild Crry labeling in photoreceptors and absent labeling in the RPE. (Blue, DAPI) Ch, choroid; GCL, ganglion cell layer; INL, inner nuclear layer; ONL, outer nuclear layer; OS, outer photoreceptor segments; S, sclera. Bar=25 μm.

C5 immunolabeling was detected in the inner plexiform layer and RPE of WT mice and in all layers of the retina and RPE of mutant mice (Figure 15, A and B). While C5b-9 complex labeling was barely detected in the retina, RPE, and choroid of WT mice fed

a high-fat diet, mutant mice showed more obvious immunolabeling throughout the outer retina, diffusely through the RPE, and minimally in the choroid (Figure 15, C and D). CD59, a regulator of C5b-9 formation, was barely detectable in WT mice, whereas in mutant mice CD59 labeling was prominent in the photoreceptor outer segments and the RPE, with relatively less staining in the choroid (Figure 15, E and F).

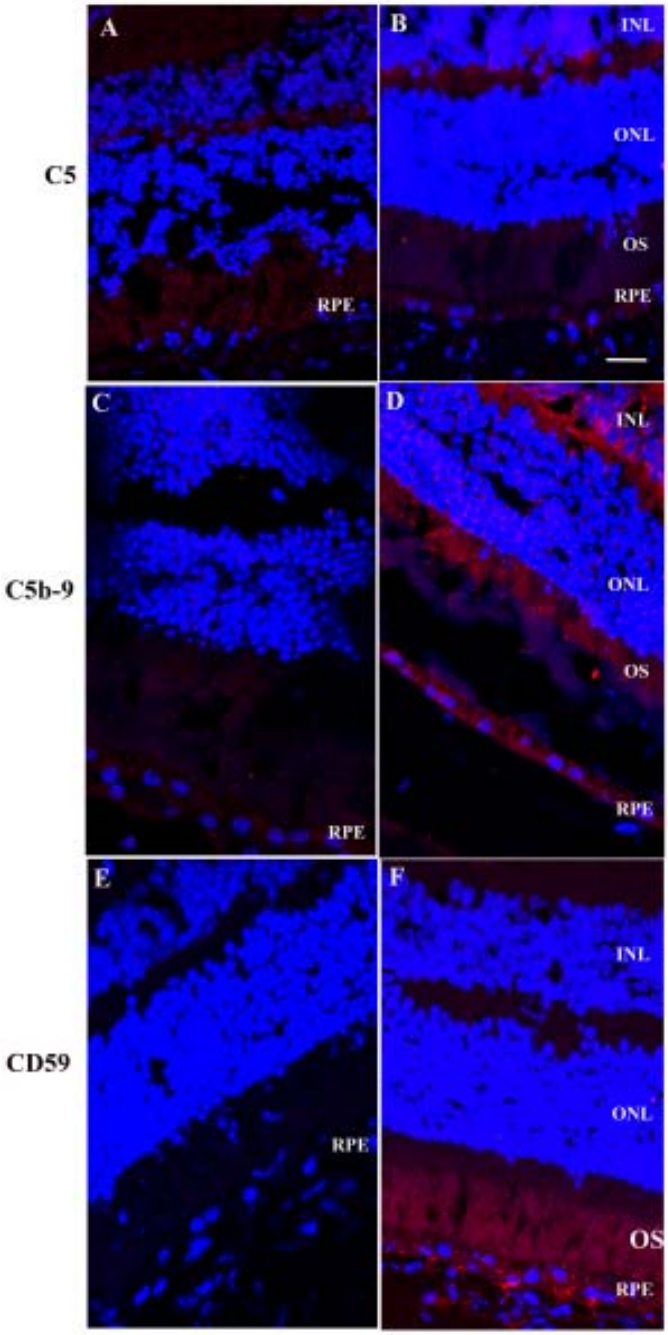

FIGURE 15

Fluorescence immunohistochemistry of C5, C5b-9, and CD59 in retinas of WT and mutant LBS$^-$ Lp(a) mice fed a high-fat diet. A, Retina from 12-month-old WT Lp(a) mouse with minimal to no immunolabeling for C5. B, Retina from 12-month-old mutant LBS$^-$ Lp(a) mouse with immunolabeling for C5 within the inner retinal layers and the retinal pigment epithelium (RPE). C, WT Lp(a) retina with minimal immunolabeling for C5b-9. D, Mutant retina with prominent labeling for C5b-9 in the outer retina and RPE. E, WT Lp(a) retina with minimal CD59 labeling. F, Mutant retina with immunolabeling in the outer photoreceptors (OS) and RPE. (Blue, DAPI) INL, inner nuclear layer; ONL, outer nuclear layer. Bar=25 μm.

ACCUMULATION OF OxPL IS NOT ASSOCIATED WITH RPE APOPTOSIS

While the ultrastructural changes are compatible with RPE degeneration, the nuclei of both WT and mutant mice given a high-fat diet appeared normal, with mild chromatin condensation as the most severe change (Figure 16, A and B). Pyknotic nuclei were not identified in either Lp(a) model. We confirmed a lack of cell death by apoptosis with absent annexin V (Figure 16, C and D) and TUNEL labeling (Figure 16, E and F). These results indicate that the RPE undergoes degeneration, but without evidence of apoptosis.

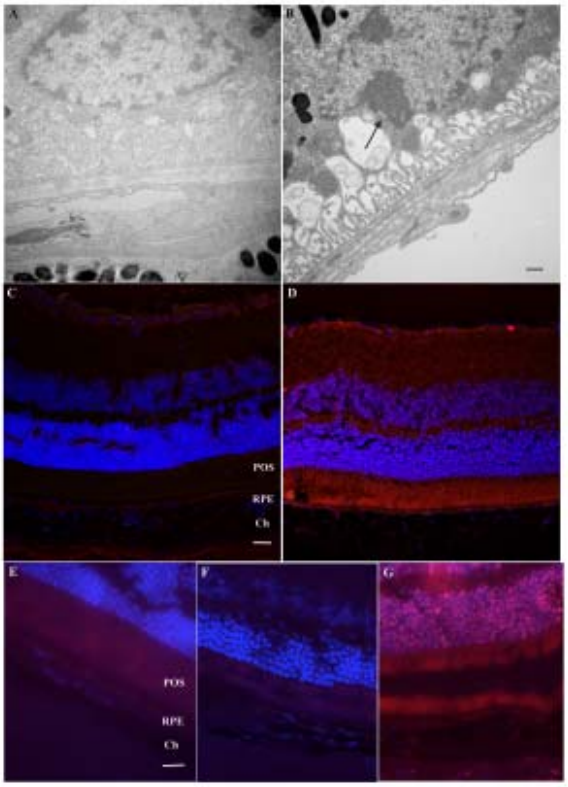

FIGURE 16

Assessment of cell death in retinas of WT and mutant LBS$^-$ Lp(a) mice fed a high-fat diet. A, Electron micrograph of a retinal pigment epithelium (RPE) cell with normal nuclei from a WT Lp(a) mouse. B, Electron micrograph of an RPE cell with mild chromatin condensation (arrow) from a mutant mouse. Bar=500 nm. C, Negative annexin V labeling (green), but mild OxPL labeling with E06 antibody (red) of a WT Lp(a) mouse. Bar=25 μm. D, Negative annexin V labeling (green) and more intense OxPL labeling (red) of a mutant mouse. E and F, Absent TUNEL labeling of retinas from WT Lp(a) mouse (E) and from mutant LBS$^-$ Lp(a) mouse (F). Bar= 25 μm. G, Positive control after DNase treatment of a retina from a WT mouse. (Red, TUNEL; Blue, DAPI) Ch, choroid; POS, photoreceptor outer segment.

DISCUSSION

Oxidized lipids, including OxPL, are proinflammatory. In humans, Lp(a) binds PC-containing OxPL and accounts for up to 85% to 90% of all OxPL detected on lipoproteins by E06 in human plasma. Utilizing the same E06 monoclonal antibody, we found that PC-containing OxPL were widely distributed throughout the fundus in both AMD and age-matched control maculas, which is a natural consequence of the known high oxidative stress environment of the macula.[61] Our immunohistochemical studies document for the first time that Lp(a) accumulates in the macula of human AMD samples, whereas our study of transgenic Lp(a) mice provides insights into the role of OxPL and Lp(a) in the fundus. Mutant LBS$^-$ Lp(a) mice, which contain an Lp(a) that does not bind OxPL that is detected by E06, when stressed with a high-fat diet, developed hallmark changes associated with AMD, including RPE cell degeneration, heterogeneous basal deposits, and drusen. These phenotypic changes were associated with increased OxPL, decreased antioxidant defenses, increased complement, and decreased complement regulators. In contrast, WT Lp(a) did not display any AMD-type changes. Together, our data suggest that the ability of Lp(a) to bind E06-detectable OxPL may play a protective role in the macula.

We found apo(a) immunolabeling in the macula that was confined mainly to the choroid and outer Bruch's membrane, and not to any great extent in the RPE, subretinal space, or retina. Importantly, apoB-100 labeling had overlapping regions with apo(a) in the choroid and Bruch's membrane, which likely represents some intact Lp(a). Apo(a), apoB-100, and OxPL immunolabeling did not always completely colocalize. This does not necessarily indicate that Lp(a) particles are not present, but rather suggests that apoB-100 could be degraded and/or removed at a greater rate, whereas apo(a) remains bound to the matrix for a longer period of time. A similar pattern of immunolabeling in which there was a wider distribution pattern of apo(a) than apoB-100 was previously reported in atherosclerotic specimens, and similarly, OxPL labeling exceeded areas of apo(a) immunolabeling.[36] The more extensive distribution of OxPL compared to apo(a) in the fundus, like that in atherosclerotic vessels, suggests that in addition to any OxPL carried by Lp(a) in the fundus, OxPL is abundantly formed in the high oxidative stress environment of the fundus. These results are similar to other reports documenting the presence of PC-containing OxPL in the fundus in AMD.[6,11] In our library, while the immunostaining of OxPL in AMD and age-matched control maculas appeared similar in intensity, the main distinction was that OxPL labeling was also in AMD lesions such as basal deposits and drusen. Immunohistochemistry is not quantitative so subtle but meaningful differences in the quantity, as well as types, of OxPL between AMD and controls could have been missed. In addition, while we added a strong lipophilic antioxidant (BHT) in the preservation of the globes, postmortem oxidation from a delay before tissue fixation could have masked any quantitative differences in OxPLs between AMD and control eyes.

The large molecular size of intact Lp(a) suggests that it would have difficulty penetrating past either the inner or outer blood-retinal barrier. In support of this theory, we found that apo(a) remained within retinal blood vessels and not in the neurosensory retina itself. Some drusen did immunolabel for apo(a) in our AMD samples. It has been known for some time that the outer blood-retinal barrier, composed in part of Bruch's membrane, is compromised in early AMD.[62] We suggest that the apo(a) in drusen is due to

breakdown of the outer barrier. ApoB-100, but not apo(a), was observed in the RPE. The localization of apoB-100 in the RPE supports our work[63] and that of the Curcio lab[18,64] that apoB can be synthesized and secreted by RPE cells. The lack of apo(a) immunolabeling in RPE cells and our inability to identify apo(a) mRNA expression by human ARPE-19 cells both suggest that the RPE is not a source of ocular apo(a), and that apo(a) likely originates from the systemic circulation. Plasma Lp(a) is thought to be assembled extracellularly in the space of Disse by the covalent attachment of apoB-100 with apo(a), as reviewed by Dieplinger and Utermann.[65] Our data in the eye raise the possibility that in a similar manner, apoB-100 could be secreted by the RPE and then bind to systemically derived apo(a) in the extracellular space to form an ocular Lp(a) particle.

Mice do not express apo(a), and therefore to generate mice that have Lp(a), one needs to express both human apo(a) and human apoB-100, as murine apoB-100 does not form a covalent link with human apo(a). We have generated two mouse Lp(a) models, one in which the Lp(a) binds OxPL, the WT LP(a) mouse, and the mutant LBS$^-$ Lp(a) mouse, in which their Lp(a) do not appear to bind significant quantities of OxPL that is recognized by E06. We examined the eyes of these two Lp(a) mouse models after they consumed either regular or high-fat diets. While few differences were found in their eyes when they consumed a normal chow diet, remarkably, considerable differences were found when they were stressed with a high-fat diet. Compared to the WT Lp(a) mice, the mutant LBS$^-$ mice accumulated considerable OxPL in the fundus over time, and further, this was associated with a low antioxidant profile, complement activation, and phenotypic markers of AMD. These findings raise the possibility that chronic accumulation of OxPLs induce a proinflammatory environment that contributes to phenotypic changes reminiscent of AMD, and further, that the ability of Lp(a) to bind OxPL may help to ameliorate the adverse effects of OxPL generated in the eye during normal aging and at an enhanced rate in response to high-oxidant stress, as occurs with the high-fat diets.

Our mouse studies lead to the suggestion that the mutant apo(a) present in the mutant LBS$^-$ Lp(a) mouse leads to chronic and enhanced retinal exposure to OxPL, which are continuously being formed even in normal settings. The exact binding characteristics of the mutant apo(a) with OxPL has not been elucidated. Intact Lp(a) consists of both LDL and apo(a), and using E06, we do not detect OxPL in the Lp(a) of mutant mice. However, using liquid chromatography–tandem mass spectrometry (LC-MS/MS), we previously found that some OxPL appear to bind to mutant apo(a)—the apo(a) component of Lp(a)—yet it is not detected by E06.[29] LC-MS/MS is highly sensitive and may pick up the presence of OxPL, but quantitatively, OxPL may be in low absolute amounts and/or cryptic to E06, leading to diminished E06 reactivity, but still able to induce stress. Our current theory is that apo(a) poorly binds OxPL so that OxPL accumulate in the fundus. In turn, the increased OxPL could stress the antioxidant, cytoprotective mechanisms of the macula. In support of this theory, we observed decreased labeling for NQO-1 and HO-1 in mutant LBS$^-$ Lp(a) transgenic mice compared to WT Lp(a) mice. The apparent paradoxical response suggests that the antioxidant response is depleted during chronic oxidative stress. We specifically selected these two antioxidant genes to test because they are activated by the master antioxidant transcription factor Nrf2,[66] which is known to be stimulated by OxPL,[67,68] because chronic oxidative stress including lipid peroxidation products has been shown to impair the Nrf2 signaling response,[67,69] and because we recently reported decreased Nrf2 in AMD specimens.[70] While we did not specifically test Nrf2 signaling itself, our results suggest an impaired antioxidant response due to enhanced chronic exposure to an OSE like OxPL. Future studies will be directed toward understanding when the antioxidant system fails and the extent that the Nrf2 signaling system is involved.

Oxidative stress can activate innate immunity through NF-κB signaling, as reviewed by Baldwin,[71] including complement.[72] Compared to WT Lp(a) mice, we found that mutant Lp(a) mice fed a high-fat diet displayed a prominent complement response mainly at C3, with less C5 and C5b-9 labeling. Our experiments also found reduced CFH, and no difference in labeling of Crry, the major cell membrane C3 regulator in mice, but robust CD59, a major regulator of C5b-9 formation. CFH is impaired by oxidative stress.[73] While Crry did not decrease, its lack of coincident increase with increased C3 in the mutant mice suggests that along with decreased CFH, it contributes to inadequate C3 regulation. Thus, oxidative stress generating OxPL, if inadequately neutralized by Lp(a), could drive complement activation through both increased complement component and impaired complement regulator abundance, particularly at C3.

The activation of C3, as suggested by C3d abundance in tissues,[74] without substantial activation of other final pathway components such as C5 and C5b-9, is compatible with generating a proinflammatory environment. For example, C3a anaphylatoxin can generate the production of proinflammatory cytokines such as the robust IL-1b,[75] which can recruit inflammatory cells, whereas C3b is a proinflammatory opsonin because it promotes IL-8 and TNF-α production by macrophages.[76] Because we identified marked phenotypic changes reminiscent of AMD, we suggest that the C3 complement response was inadequately controlled, and converted the normally protective response into a pathologic one. While C5b-9 complexes were formed, we were unable to determine the extent that C5b-9 was regulated by CD59, and whether the amount of C5b-9 formation was able to induce vascular endothelial growth factor production,[73] activate the inflammasome,[77] or induce cell lysis of the RPE. While C5b-9 can also induce apoptosis, as reviewed in Cole and Morgan,[78] we did not observe any evidence of this process.

The distinction between aging changes and early AMD can be subtle and is a continuum. The most compelling histopathological changes associated with early AMD include drusen and thick, heterogeneous basal laminar deposits, located between the RPE cell and its basement membrane, or basal linear deposits, which are accumulations within the inner collagenous layer in Bruch's membrane,[26,79] as well as RPE degenerative changes such as truncated and fewer basal infoldings[45,50] and cytoplasmic membranous vacuoles, especially when overlying drusen.[48] While no mouse model has been found to mimic AMD, we found compelling, specific changes that are associated with AMD in the mutant LBS$^-$ Lp(a) mice. These include RPE vacuoles seen on light microscopy that corresponded nicely with the marked membranous vacuoles seen on transmission electron microscopy (TEM), and the truncated and fewer basal infoldings of the RPE. In Bruch's membrane, we observed basal laminar deposits that were heterogeneous in composition.

Since drusen are rarely seen in mice, perhaps the most impressive phenotypic change in mutant LBS$^-$ Lp(a) mice was the identification of drusen in 40% of eyes examined by light microscopy, which was confirmed by TEM. Our experimental strategy was to stress these mice with a high-cholesterol diet in order to test the Lp(a) response. Epidemiological studies indicate a high-fat diet is a weak risk factor for AMD.[80] To determine if mutant LBS$^-$ Lp(a) mice will develop more drusen compared to WT Lp(a) mice, in the future we want to expose these mice to greater risk factors, such as increased age or long-term exposure to cigarette smoke, since aging and cigarette smoking are the two strongest epidemiological risk factors for AMD. We, of course, recognize that the demonstration of similar biochemical and morphological changes in these mutant mice does not prove that similar processes occur in humans to cause AMD, but we feel that these observations suggest novel hypotheses that can lead to informative new studies in humans.

We propose that OxPL formed during the normal metabolism of photoreceptors are processed by the normal phagocytosis of outer segments by the RPE and are eventually released basally toward the choriocapillaris. Because Lp(a) is sufficiently large that it cannot penetrate past an intact Bruch's membrane, systemically derived Lp(a) will bind and "neutralize" OxPL that are processed to the choriocapillaris. Mutant Lp(a) mice, whose Lp(a) does not appear to be capable of binding significant quantities of OxPL, or at least sufficient OxPL to be recognizable by E06, would therefore not be able to equally bind and neutralize these OxPL—at least when compared to WT Lp(a) mice. Consequently, aging-related changes to Bruch's membrane, such as AGE formation[81] and accumulation of lipoproteins,[17,18] could impair the essential diffusion of OxPL across Bruch's membrane, which would result in their accumulation. Breakdown of Bruch's membrane, a known change in AMD, could even allow some penetration of Lp(a) into Bruch's membrane, as we observed in drusen deposits. Just as accumulation of Lp(a) in the subendothelial matrix in atherosclerosis results in local immune activation, likewise, Lp(a) particles that accumulate within Bruch's membrane could result in a source of OxPL that chronically activates innate immunity and results in either RPE cell injury or drusen formation. Future experiments will be designed to address this theory.

ACKNOWLEDGMENTS

Funding/Support: This work was supported by grants EY14005 (J.T.H.) and EY019904 (J.T.H.) from the National Institutes of Health/National Eye Institute; a Beckman Foundation AMD grant (J.T.H.); the Thome Foundation (J.T.H.); a Research to Prevent Blindness (RPB) Senior Scientist Award (J.T.H.); Core Grants P30EY001765 and HL 088093 from the National Institutes of Health (J.L.W. and S.T.); the Robert Bond Welch Professorship (J.T.H.); a gift from the Merlau family; and an Unrestricted Grant from RPB to the Wilmer Eye Institute. Some funding was provided by the Swiss National Science Foundation (PBBSP3-124742) and the Swiss Academy of Medical Sciences (PASMP3_132566).

Financial Disclosures: Dr Tsimikas and Dr Witztum are coinventors of and receive royalties from patents on oxidation-specific antibodies owned by the University of California San Diego (UCSD). Dr Witztum is a consultant to Isis Pharmaceuticals, Intercept Pharmaceuticals, and Cymabay Inc. Dr Tsimikas has dual employment at UCSD and Isis Pharmaceuticals. The other authors have no disclosures.

Author Contributions: Design and conduct of study (J.T.H.); Collection and management of data (J.T.H., M.T., K.E., G.L., A.J.); Analysis and interpretation of data (J.T.H., J.W., S.T.); Preparation, review, and approval of manuscript (J.T.H., M.T., K.E., G.L., A.J., J.W., S.T.).

REFERENCES

1. Miller YI, Choi SH, Wiesner P, et al. Oxidation-specific epitopes are danger-associated molecular patterns recognized by pattern recognition receptors of innate immunity. *Circ Res* 2011;108(2):235-248.
2. Chou MY, Hartvigsen K, Hansen LF, et al. Oxidation-specific epitopes are important targets of innate immunity. *J Intern Med* 2008;263(5):479-488.
3. Binder CJ, Hartvigsen K, Chang MK, et al. IL-5 links adaptive and natural immunity specific for epitopes of oxidized LDL and protects from atherosclerosis. *J Clin Invest* 2004;114(3):427-437.
4. Weismann D, Hartvigsen K, Lauer N, et al. Complement factor H binds malondialdehyde epitopes and protects from oxidative stress. *Nature* 2011;478(7367):76-81.
5. Gu X, Meer SG, Miyagi M, et al. Carboxyethylpyrrole protein adducts and autoantibodies, biomarkers for age-related macular degeneration. *J Biol Chem* 2003;278(43):42027-42035.
6. Sun M, Finnemann SC, Febbraio M, et al. Light-induced oxidation of photoreceptor outer segment phospholipids generates ligands for CD36-mediated phagocytosis by retinal pigment epithelium: a potential mechanism for modulating outer segment phagocytosis under oxidant stress conditions. *J Biol Chem* 2006;281(7):4222-4230.
7. Schutt F, Ueberle B, Schnolzer M, Holz FG, Kopitz J. Proteome analysis of lipofuscin in human retinal pigment epithelial cells. *FEBS Lett* 2002;528(1-3):217-221.
8. Schutt F, Bergmann M, Holz FG, Kopitz J. Proteins modified by malondialdehyde, 4-hydroxynonenal, or advanced glycation end products in lipofuscin of human retinal pigment epithelium. *Invest Ophthalmol Vis Sci* 2003;44(8):3663-3668.
9. Farboud B, Aotaki-Keen A, Miyata T, Hjelmeland LM, Handa JT. Development of a polyclonal antibody with broad epitope specificity for advanced glycation endproducts and localization of these epitopes in Bruch's membrane of the aging eye. *Mol Vis* 1999;5:11.

10. Crabb JW, Miyagi M, Gu X, et al. Drusen proteome analysis: an approach to the etiology of age-related macular degeneration. *Proc Natl Acad Sci U S A* 2002;99(23):14682-14687.
11. Suzuki M, Kamei M, Itabe H, et al. Oxidized phospholipids in the macula increase with age and in eyes with age-related macular degeneration. *Mol Vis* 2007;13:772-778.
12. Chang MK, Binder CJ, Miller YI, et al. Apoptotic cells with oxidation-specific epitopes are immunogenic and proinflammatory. *J Exp Med* 2004;200(11):1359-1370.
13. Shaw PX, Horkko S, Chang MK, et al. Natural antibodies with the T15 idiotype may act in atherosclerosis, apoptotic clearance, and protective immunity. *J Clin Invest* 2000;105(12):1731-1740.
14. Friedman P, Horkko S, Steinberg D, Witztum JL, Dennis EA. Correlation of antiphospholipid antibody recognition with the structure of synthetic oxidized phospholipids. Importance of Schiff base formation and aldol condensation. *J Biol Chem* 2002;277(9):7010-7020.
15. Curcio CA, Millican CL, Bailey T, Kruth HS. Accumulation of cholesterol with age in human Bruch's membrane. *Invest Ophthalmol Vis Sci* 2001;42(1):265-274.
16. Curcio CA, Presley JB, Malek G, Medeiros NE, Avery DV, Kruth HS. Esterified and unesterified cholesterol in drusen and basal deposits of eyes with age-related maculopathy. *Exp Eye Res* 2005;81(6):731-741.
17. Li CM, Chung BH, Presley JB, et al. Lipoprotein-like particles and cholesteryl esters in human Bruch's membrane: initial characterization. *Invest Ophthalmol Vis Sci* 2005;46(7):2576-2586.
18. Malek G, Li CM, Guidry C, Medeiros NE, Curcio CA. Apolipoprotein B in cholesterol-containing drusen and basal deposits of human eyes with age-related maculopathy. *Am J Pathol* 2003;162(2):413-425.
19. Yamada Y, Tian J, Yang Y, et al. Oxidized low density lipoproteins induce a pathologic response by retinal pigmented epithelial cells. *J Neurochem* 2008;105(4):1187-1197.
20. Glass CK, Witztum JL. Atherosclerosis: the road ahead. *Cell* 2001;104(4):503-516.
21. Dube JB, Boffa MB, Hegele RA, Koschinsky ML. Lipoprotein(a): more interesting than ever after 50 years. *Curr Opin Lipidol* 2012;23(2):133-140.
22. Kronenberg F, Utermann G. Lipoprotein(a): resurrected by genetics. *J Intern Med* 2013;273(1):6-30.
23. Hoover-Plow J, Huang M. Lipoprotein(a) metabolism: potential sites for therapeutic targets. *Metabolism* 2013;62(4):479-491.
24. McLean JW, Tomlinson JE, Kuang WJ, et al. cDNA sequence of human apolipoprotein(a) is homologous to plasminogen. *Nature* 1987;330(6144):132-137.
25. Bergmark C, Dewan A, Orsoni A, et al. A novel function of lipoprotein [a] as a preferential carrier of oxidized phospholipids in human plasma. *J Lipid Res* 2008;49(10):2230-2239.
26. Sarks SH. Ageing and degeneration in the macular region: a clinico-pathological study. *Br J Ophthalmol* 1976;60(5):324-341.
27. Yamada Y, Ishibashi K, Ishibashi K, et al. The expression of advanced glycation endproduct receptors in rpe cells associated with basal deposits in human maculas. *Exp Eye Res* 2006;82(5):840-848.
28. Dunn KC, Aotaki-Keen AE, Putkey FR, Hjelmeland LM. ARPE-19, a human retinal pigment epithelial cell line with differentiated properties. *Exp Eye Res* 1996;62(2):155-169.
29. Leibundgut G, Scipione C, Yin H, et al. Determinants of binding of oxidized phospholipids on apolipoprotein (a) and lipoprotein (a). *J Lipid Res* 2013;54(10):2815-2830.
30. Mulichak AM, Tulinsky A, Ravichandran KG. Crystal and molecular structure of human plasminogen kringle 4 refined at 1.9-A resolution. *Biochemistry* 1991;30(43):10576-10588.
31. Schneider M, Witztum JL, Young SG, et al. High-level lipoprotein [a] expression in transgenic mice: evidence for oxidized phospholipids in lipoprotein [a] but not in low density lipoproteins. *J Lipid Res* 2005;46(4):769-778.
32. Skalen K, Gustafsson M, Rydberg EK, et al. Subendothelial retention of atherogenic lipoproteins in early atherosclerosis. *Nature* 2002;417(6890):750-754.
33. Merki E, Graham M, Taleb A, et al. Antisense oligonucleotide lowers plasma levels of apolipoprotein (a) and lipoprotein (a) in transgenic mice. *J Am Coll Cardiol* 2011;57(15):1611-1621.
34. Merki E, Graham MJ, Mullick AE, et al. Antisense oligonucleotide directed to human apolipoprotein B-100 reduces lipoprotein(a) levels and oxidized phospholipids on human apolipoprotein B-100 particles in lipoprotein(a) transgenic mice. *Circulation* 2008;118(7):743-753.
35. Taleb A, Witztum JL, Tsimikas S. Oxidized phospholipids on apoB-100-containing lipoproteins: a biomarker predicting cardiovascular disease and cardiovascular events. *Biomark Med* 2011;5(5):673-694.
36. van Dijk RA, Kolodgie F, Ravandi A, et al. Differential expression of oxidation-specific epitopes and apolipoprotein(a) in progressing and ruptured human coronary and carotid atherosclerotic lesions. *J Lipid Res* 2012;53(12):2773-2790.
37. Fefer P, Tsimikas S, Segev A, et al. The role of oxidized phospholipids, lipoprotein (a) and biomarkers of oxidized lipoproteins in chronically occluded coronary arteries in sudden cardiac death and following successful percutaneous revascularization. *Cardiovasc Revasc Med* 2012;13(1):11-19.
38. Tsimikas S, Kiechl S, Willeit J, et al. Oxidized phospholipids predict the presence and progression of carotid and femoral atherosclerosis and symptomatic cardiovascular disease: five-year prospective results from the Bruneck study. *J Am Coll Cardiol* 2006;47(11):2219-2228.

39. Kiechl S, Willeit J, Mayr M, et al. Oxidized phospholipids, lipoprotein(a), lipoprotein-associated phospholipase A2 activity, and 10-year cardiovascular outcomes: prospective results from the Bruneck study. *Arterioscler Thromb Vasc Biol* 2007;27(8):1788-1795.
40. Cousins SW, Espinosa-Heidmann DG, Alexandridou A, Sall J, Dubovy S, Csaky K. The role of aging, high fat diet and blue light exposure in an experimental mouse model for basal laminar deposit formation. *Exp Eye Res* 2002;75(5):543-553.
41. Ida H, Ishibashi K, Reiser K, Hjelmeland LM, Handa JT. Ultrastructural aging of the RPE-Bruch's membrane-choriocapillaris complex in the D-galactose-treated mouse. *Invest Ophthalmol Vis Sci* 2004;45(7):2348-2354.
42. Ananth CV, Kleinbaum DG. Regression models for ordinal responses: a review of methods and applications. *Int J Epidemiol* 1997;26(6):1323-1333.
43. Kagawa A, Azuma H, Akaike M, Kanagawa Y, Matsumoto T. Aspirin reduces apolipoprotein(a) (apo(a)) production in human hepatocytes by suppression of apo(a) gene transcription. *J Biol Chem* 1999;274(48):34111-34115.
44. Franceschini A, Capece M, Chiozzi P, et al. The P2X7 receptor directly interacts with the NLRP3 inflammasome scaffold protein. *FASEB J* 2015;29(6):2450-2461.
45. Olsen TS, Wassef NF, Olsen HS, Hansen HE. Ultrastructure of the kidney in acute interstitial nephritis. *Ultrastruct Pathol* 1986;10(1):1-16.
46. Olsen S, Burdick JF, Keown PA, Wallace AC, Racusen LC, Solez K. Primary acute renal failure ("acute tubular necrosis") in the transplanted kidney: morphology and pathogenesis. *Medicine (Baltimore)* 1989;68(3):173-187.
47. Drueke T, Hennessen U, Nabarra B, et al. Ultrastructural and functional abnormalities of intestinal and renal epithelium in the SHR. *Kidney Int* 1990;37(6):1438-1448.
48. Anderson DH, Mullins RF, Hageman GS, Johnson LV. A role for local inflammation in the formation of drusen in the aging eye. *Am J Ophthalmol* 2002;134(3):411-431.
49. van der Schaft TL, de Bruijn WC, Mooy CM, Ketelaars DA, de Jong PT. Is basal laminar deposit unique for age-related macular degeneration? *Arch Ophthalmol* 1991;109(3):420-425.
50. Green WR, Enger C. Age-related macular degeneration histopathologic studies. The 1992 Lorenz E. Zimmerman Lecture. *Ophthalmology* 1993;100(10):1519-1535.
51. Landa G, Su E, Garcia PM, Seiple WH, Rosen RB. Inner segment-outer segment junctional layer integrity and corresponding retinal sensitivity in dry and wet forms of age-related macular degeneration. *Retina* 2011;31(2):364-370.
52. Thimmulappa RK, Lee H, Rangasamy T, et al. Nrf2 is a critical regulator of the innate immune response and survival during experimental sepsis. *J Clin Invest* 2006;116(4):984-995.
53. Hageman GS, Anderson DH, Johnson LV, et al. A common haplotype in the complement regulatory gene factor H (HF1/CFH) predisposes individuals to age-related macular degeneration. *Proc Natl Acad Sci U S A* 2005;102(20):7227-7232.
54. Edwards AO, Ritter R 3rd, Abel KJ, Manning A, Panhuysen C, Farrer LA. Complement factor H polymorphism and age-related macular eegeneration. *Science* 2005;308(5720):421-424.
55. Haines JL, Hauser MA, Schmidt S, et al. Complement factor H variant increases the risk of age-related macular degeneration. *Science* 2005;308(5720):419-421.
56. Klein RJ, Zeiss C, Chew EY, et al. Complement factor H polymorphism in age-related macular degeneration. *Science* 2005;308(5720):385-389.
57. Yates JR, Sepp T, Matharu BK, et al. Complement C3 variant and the risk of age-related macular degeneration. *N Engl J Med* 2007;357(6):553-561.
58. Maller JB, Fagerness JA, Reynolds RC, Neale BM, Daly MJ, Seddon JM. Variation in complement factor 3 is associated with risk of age-related macular degeneration. *Nat Genet* 2007;39(10):1200-1201.
59. Gold B, Merriam JE, Zernant J, et al. Variation in factor B (BF) and complement component 2 (C2) genes is associated with age-related macular degeneration. *Nat Genet* 2006;38(4):458-462.
60. Kondo N, Bessho H, Honda S, Negi A. Additional evidence to support the role of a common variant near the complement factor I gene in susceptibility to age-related macular degeneration. *Eur J Hum Genet* 2010;18(6):634-635.
61. Winkler BS, Boulton ME, Gottsch JD, Sternberg P. Oxidative damage and age-related macular degeneration. *Mol Vis* 1999;5:32.
62. Merin S, Blair NP, Tso MO. Vitreous fluorophotometry in patients with senile macular degeneration. *Invest Ophthalmol Vis Sci* 1987;28(4):756-759.
63. Wu T, Tian J, Cutler RG, et al. Knockdown of FABP5 mRNA decreases cellular cholesterol levels and results in decreased apoB100 secretion and triglyceride accumulation in ARPE-19 cells. *Lab Invest* 2010;90(6):963-965.
64. Li CM, Presley JB, Zhang X, et al. Retina expresses microsomal triglyceride transfer protein: implications for age-related maculopathy. *J Lipid Res* 2005;46(4):628-640.
65. Dieplinger H, Utermann G. The seventh myth of lipoprotein(a): where and how is it assembled? *Current Opin Lipidol* 1999;10(3):275-283.
66. Rangasamy T, Cho CY, Thimmulappa RK, et al. Genetic ablation of Nrf2 enhances susceptibility to cigarette smoke-induced emphysema in mice. *J Clin Invest* 2004;114(9):1248-1259.
67. Kadl A, Meher AK, Sharma PR, et al. Identification of a novel macrophage phenotype that develops in response to atherogenic phospholipids via Nrf2. *Circ Res* 2010;107(6):737-746.

68. Thimmulappa RK, Gang X, Kim JH, Sussan TE, Witztum JL, Biswal S. Oxidized phospholipids impair pulmonary antibacterial defenses: evidence in mice exposed to cigarette smoke. *Biochem Biophys Res Commun* 2012;426(2):253-259.
69. Suzuki M, Betsuyaku T, Ito Y, et al. Down-regulated NF-E2-related factor 2 in pulmonary macrophages of aged smokers and patients with chronic obstructive pulmonary disease. *Am J Respir Cell Mol Biol* 2008;38(6):673-682.
70. Wang L, Kondo N, Cano M, et al. Nrf2 signaling modulates cigarette smoke-induced complement activation in retinal pigmented epithelial cells. *Free Radic Biol Med* 2014;70:155-166.
71. Baldwin AS Jr. The NF-kappa B and I kappa B proteins: new discoveries and insights. *Ann Rev Immunol* 1996;14:649-683.
72. Shavva VS, Mogilenko DA, Dizhe EB, Oleinikova GN, Perevozchikov AP, Orlov SV. Hepatic nuclear factor 4alpha positively regulates complement C3 expression and does not interfere with TNFalpha-mediated stimulation of C3 expression in HepG2 cells. *Gene* 2013;524(2):187-192.
73. Thurman JM, Renner B, Kunchithapautham K, et al. Oxidative stress renders retinal pigment epithelial cells susceptible to complement-mediated injury. *J Biol Chem* 2009;284(25):16939-16947.
74. Thurman JM, Kulik L, Orth H, et al. Detection of complement activation using monoclonal antibodies against C3d. *J Clin Invest* 2013;123(5):2218-2230.
75. Monsinjon T, Gasque P, Chan P, Ischenko A, Brady JJ, Fontaine MC. Regulation by complement C3a and C5a anaphylatoxins of cytokine production in human umbilical vein endothelial cells. *FASEB J* 2003;17(9):1003-1014.
76. Amarilyo G, Verbovetski I, Atallah M, et al. iC3b-opsonized apoptotic cells mediate a distinct anti-inflammatory response and transcriptional NF-kappaB-dependent blockade. *Eur J Immunol* 2010;40(3):699-709.
77. Laudisi F, Spreafico R, Evrard M, et al. Cutting edge: The NLRP3 inflammasome links complement-mediated inflammation and IL-1beta release. *J Immunol* 2013;191(3):1006-1010.
78. Cole DS, Morgan BP. Beyond lysis: how complement influences cell fate. *Clin Sci* 2003;104(5):455-466.
79. van der Schaft TL, Mooy CM, de Bruijn WC, Bosman FT, de Jong PT. Immunohistochemical light and electron microscopy of basal laminar deposit. *Graefes Arch Clin Exp Ophthalmol* 1994;232(1):40-46.
80. Seddon JM, Cote J, Rosner B. Progression of age-related macular degeneration: association with dietary fat, transunsaturated fat, nuts, and fish intake. *Arch Ophthalmol* 2003;121(12):1728-1737.
81. Handa JT, Verzijl N, Matsunaga H, et al. Increase in the advanced glycation end product pentosidine in Bruch's membrane with age. *Invest Ophthalmol Vis Sci* 1999;40(3):775-779.